Article

Cell division protein FtsK coordinates bacterial chromosome segregation and daughter cell separation in *Staphylococcus aureus*

Helena Veiga[1,*] , Ambre Jousselin[1,†] , Simon Schäper[1], Bruno M Saraiva[1] , Leonor B Marques[1], Patricia Reed[1], Joana Wilton[1,‡] , Pedro M Pereira[1] , Sérgio R Filipe[1,2] & Mariana G Pinho[1,**]

Abstract

Unregulated cell cycle progression may have lethal consequences and therefore, bacteria have various mechanisms in place for the precise spatiotemporal control of cell cycle events. We have uncovered a new link between chromosome replication/segregation and splitting of the division septum. We show that the DNA translocase domain-containing divisome protein FtsK regulates cellular levels of a peptidoglycan hydrolase Sle1, which is involved in cell separation in the bacterial pathogen *Staphylococcus aureus*. FtsK interacts with a chaperone (trigger factor, TF) and establishes a FtsK-dependent TF concentration gradient that is higher in the septal region. Trigger factor binds Sle1 and promotes its preferential export at the septal region, while also preventing Sle1 degradation by the ClpXP proteolytic machinery. Upon conditions that lead to paused septum synthesis, such as DNA damage or impaired DNA replication/segregation, TF gradient is dissipated and Sle1 levels are reduced, thus halting premature septum splitting.

Introduction

During the cell cycle, bacterial cells double their mass, replicate and segregate their chromosome, and synthesize the division septum, which is then split to generate two daughter cells. While several checkpoints are well-studied in the eukaryotic cell cycle, much less is known about the cell cycle regulation in bacteria. One exception is the well-studied SOS response, which is triggered upon DNA damage and leads to cell cycle arrest via inhibition of polymerization of the cell division protein FtsZ (Mukherjee *et al*, 1998) or targeting of later divisome proteins, including FtsW (Modell *et al*, 2011; Bojer *et al*, 2019). FtsZ is one of the early divisome members that assemble at the future division site to form the so-called Z-ring and recruit later divisome proteins, including proteins required for peptidoglycan synthesis, to enable septum formation (Bi & Lutkenhaus, 1991; den Blaauwen *et al*, 2017). In some bacteria, such as *Escherichia coli*, septum synthesis is concomitant with septum splitting, leading to invagination at the division site during cytokinesis (Goehring & Beckwith, 2005). In other bacteria, such as *Bacillus subtilis* or *Staphylococcus aureus*, synthesis of the septum is completed prior to initiation of septum splitting, required for daughter cell separation (Goehring & Beckwith, 2005). The activity of peptidoglycan hydrolases that promote septum splitting has to be under tight spatiotemporal regulation, to avoid lysis-inducing breaches in the peptidoglycan network. One strategy adopted by different bacterial species is to recruit specific peptidoglycan hydrolases, or their activators, to the division septum, restricting their activity to septal peptidoglycan (Vollmer *et al*, 2008; Uehara *et al*, 2010; Sham *et al*, 2011; Bartual *et al*, 2014; Egan *et al*, 2020).

In the bacterial pathogen *S. aureus*, septum splitting is extremely fast, occurring in less than 2 ms (Monteiro *et al*, 2015; Zhou *et al*, 2015). It is therefore probable that initiation of daughter cell separation is highly controlled, to avoid premature splitting of the division septum before its completion. This is likely to be particularly important in bacterial pathogens that require numerous cell surface virulence factors that contribute to immune evasion, such as the capsular polysaccharide or cell wall-anchored surface proteins. Premature septum splitting could expose an immature cell surface, leading to clearance of bacterial cells from the infected host.

We and others have previously shown that the peptidoglycan hydrolase Sle1, an *N*-acetylmuramyl-L-alanine amidase that removes pentapeptides from glycan strands, is critical for daughter cell splitting in *S. aureus*, as its absence results in the formation of clusters of cells

1 Instituto de Tecnologia Química e Biológica António Xavier, Universidade Nova de Lisboa, Oeiras, Portugal
2 UCIBIO-REQUIMTE, Departamento de Ciências da Vida, Faculdade de Ciências e Tecnologia, Universidade Nova de Lisboa, Caparica, Portugal
*Corresponding author. Tel: +351 214469545; E-mail: hveiga@itqb.unl.pt
**Corresponding author. Tel: +351 214469545; E-mail: mgpinho@itqb.unl.pt
†Present address: Laboratoire de Microbiologie et Génétique Moléculaires, Centre de Biologie Integrative, Paul Sabatier University, Toulouse, France
‡Present address: i3S: Instituto de Investigação e Inovação em Saúde, Universidade do Porto, Porto, Portugal

(Kajimura *et al*, 2005; Monteiro *et al*, 2015). However, the mechanisms for its precise regulation in time and space remain unknown. Here, we screened for regulators of the autolysin Sle1 to identify a possible checkpoint in the *S. aureus* cell cycle controlling daughter cell separation. We found that the DNA translocase and divisome protein FtsK (Sherratt *et al*, 2010; Crozat *et al*, 2014; Veiga & Pinho, 2017) is required for the correct and timely localization of Sle1 peptidoglycan hydrolase at the division septum, delaying daughter cell separation upon DNA damage. This represents an additional level of regulation of the bacterial cell cycle, linking an early event, DNA replication and segregation, to the latest event, the separation of the two daughter cells.

Results

FtsK is required for Sle1 presence at the cell surface

The peptidoglycan hydrolase Sle1 is critical for the process of septum splitting in *S. aureus*, and its absence leads to a delay in cell cycle progression (Monteiro *et al*, 2015). Sle1 is active on the outer surface of cells, to where it is targeted via its three peptidoglycan-binding LysM domains (Frankel & Schneewind, 2012). In agreement with its role in septum splitting, immunofluorescence microscopy of intact *S. aureus* cells showed that surface Sle1 is enriched at midcell, including at recently split septa (Appendix Fig S1). To identify regulators of septum splitting, we looked for mutants lacking Sle1 at the outer surface of the cell. For this, we constructed a translational fusion between Sle1 and the *S. aureus* PhoB alkaline phosphatase, lacking its native export signal peptide, and expressed the fusion in the background of a *S. aureus phoB* deletion mutant, from the *sle1* locus. PhoB is enzymatically active only when it has been transported across the cellular membrane, and alkaline phosphatase fusions have been used to study the topology of transmembrane proteins or to identify secreted proteins in various bacteria (Manoil *et al*, 1990; Gibson & Caparon, 2002; Liu *et al*, 2015). PhoB-active colonies can be visually detected as blue colonies on plates containing the chromogenic alkaline phosphatase substrate 5-Bromo-4-chloro-3-indolyl phosphate (BCIP), while PhoB-inactive colonies appear as white. We generated mutants in the background of the COLΔ*phoB* Sle1-PhoB strain using a phage-based *mariner* transposition system (Wang *et al*, 2011). Screening of 12,000 colonies identified 15 white or pale blue colonies that likely lacked cell wall attached Sle1-PhoB. Sequencing of the transposon insertion site in these mutants showed that four had a transposon insertion in the *sle1-phoB* gene, validating the screen. Six additional mutants had transposon insertions in *secDF*, indicating that Sle1 is likely exported via the Sec system, in agreement with the fact that Sle1 has a canonical Sec signal peptide (Heilmann *et al*, 2005; Kajimura *et al*, 2005; Crane & Randall, 2017). Surprisingly, the other five mutants all had a transposon insertion in the *ftsK* gene (Fig 1A). FtsK is one of the two staphylococcal proteins with a DNA translocase domain, the other one being SpoIIIE, which are required for correct chromosome segregation (Veiga & Pinho, 2017). In *E. coli*, FtsK is a large 1,329-amino-acid protein, recruited to the divisome soon after FtsZ, which couples the last stages of chromosome segregation and cell division (Sherratt *et al*, 2010; Crozat *et al*, 2014; Levin & Janakiraman, 2021). Its N-terminal transmembrane domain is required for cell division as it interacts with other divisome proteins and is connected, via a long linker, to the C-terminal domain that has DNA translocase activity (Sherratt *et al*, 2010; Stouf

et al, 2013; Crozat *et al*, 2014). This activity is particularly important in cells that contain chromosome dimers or catenates, where FtsK activates XerCD-mediated recombination to resolve the chromosome dimers and allow chromosome segregation into the daughter cells to be successfully completed (Aussel *et al*, 2002).

Staphylococcus aureus FtsK, similarly to *B. subtilis* SftA (Biller & Burkholder, 2009; Kaimer *et al*, 2009; Saaki *et al*, 2022), does not have membrane-spanning domains, but localizes as a ring at the leading edge of the division septum, similarly to other divisome proteins (Veiga & Pinho, 2017). Its N-terminal domain has an unknown function that is independent of its DNA translocase domain, as deletion of the complete *ftsK* gene results in severe morphological and cell division defects, including the presence of clusters of cells, which are not observed in a mutant lacking only the C-terminal domain (Veiga & Pinho, 2017).

FtsK and Sle1 mutants share similar phenotypes

The cell cycle of *S. aureus* has been described as divided in three phases (Monteiro *et al*, 2015): phase 1 cells have not initiated septum synthesis; phase 2 cells are undergoing septum synthesis; and phase 3 cells have a complete septum undergoing maturation prior to splitting to generate two identical daughter cells. The delay in cell splitting in an Sle1 mutant has previously been shown to impair the progression of the cell cycle, resulting in an increase in the frequency of cells in phase 3, equating to a longer time spent in this phase (Monteiro *et al*, 2015). Consistent with a possible role of FtsK in Sle1 regulation, null mutants lacking *ftsK*, constructed in the background of two different *S. aureus* strains (8325-4Δ*ftsK* and COLΔ*ftsK*), had similar phenotypes to *sle1* mutants (8325-4Δ*sle1* and COLΔ*sle1*), namely cell splitting defects, with the presence of tetrads of cells, and a longer phase 3 (Fig 1B and C, and Appendix Fig S2). This indicates impairment in the transition from phase 3 to phase 1, which requires septum splitting. This is not due to lack of the FtsK DNA translocase domain, as deletion of the C-terminal domain of FtsK or inactivation of the DNA motor by mutation of a conserved lysine of the Walker A motif (K971A; Bigot *et al*, 2004; Kaimer *et al*, 2009; Veiga & Pinho, 2017) did not result in any obvious morphological defects (Appendix Fig S3), in agreement with our previous data (Veiga & Pinho, 2017). Moreover, addition of purified Sle1 protein to either 8325-4Δ*ftsK* or 8325-4Δ*sle1*, or to the equivalent COL mutants, reduced the frequency of tetrads and the frequency of phase 3 cells, although the latter remained higher than in the parental strain NCTC8325-4 (Fig 1C and D, and Appendix Fig S2), indicating that cell splitting defects of the FtsK mutant are mediated by lack of Sle1 at the external surface of bacteria, but that external addition of Sle1 does not result in normal cell cycle progression.

Electron microscopy images of both the FtsK and Sle1 mutants showed pairs of cells connected by a complete septum, each undergoing a second round of division (Fig 1E), confirming that the observed tetrads result from delayed splitting of daughter cells, allowing a second round of division to initiate before separation of the previous pair of daughter cells.

Sle1 is absent from all cellular compartments in the absence of FtsK

The results from the screening mentioned above suggest that Sle1 is not present on the outer surface of an FtsK mutant. We confirmed
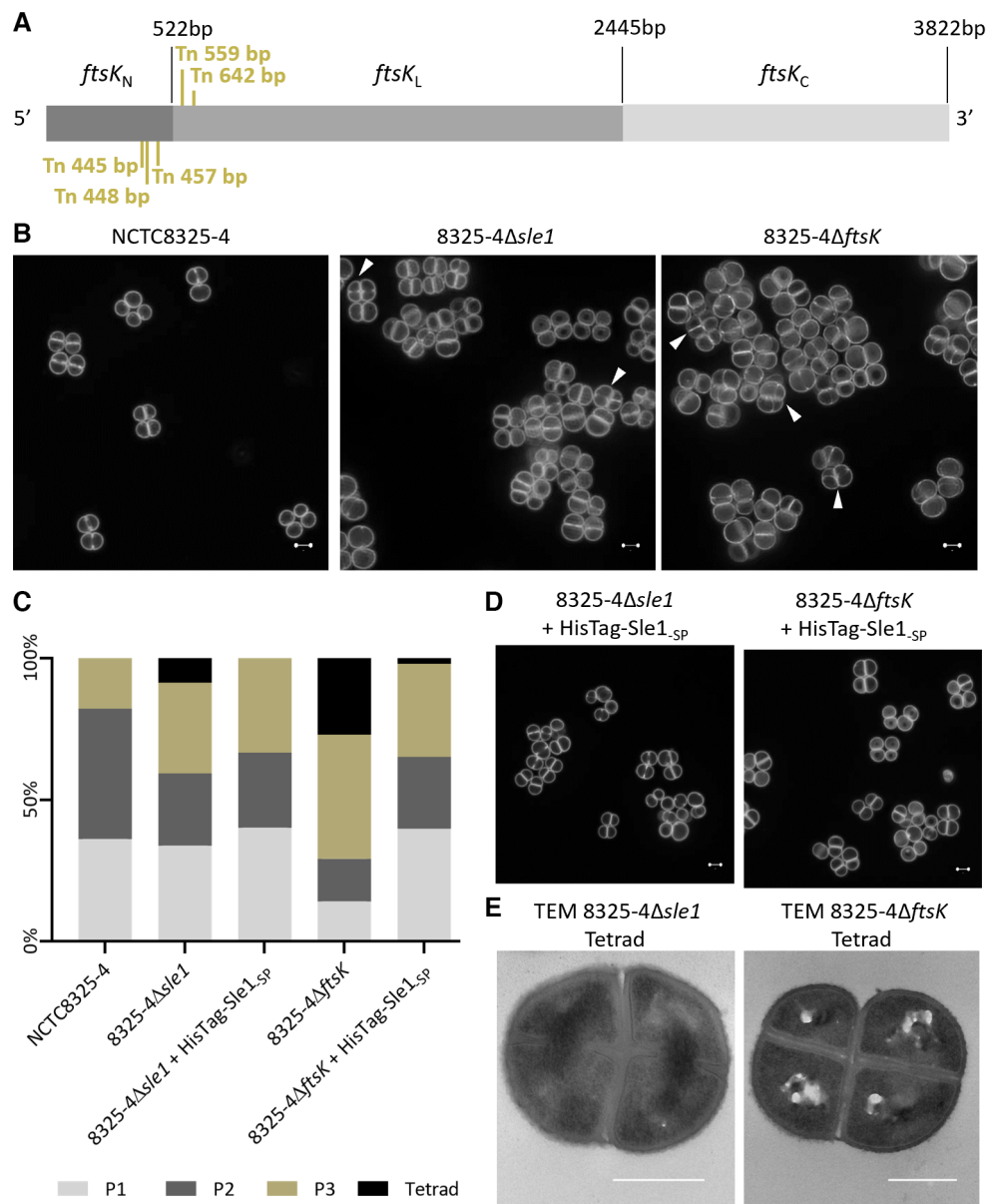
Figure 1. Lack of *S. aureus* FtsK results in the absence of Sle1 at the cell surface, impairing cell splitting.

A Schematic representation of *S. aureus ftsK* gene, with regions that encode FtsK N-terminal, Linker and C-terminal domains. A screening for Sle1 regulators identified five *ftsK* transposon mutants lacking surface Sle1-PhoB, whose transposon insertion sites are indicated in dark yellow.

B Structured Illumination Microscopy (SIM) images of *S. aureus* cells labeled with the membrane dye Nile Red. White arrowheads point to tetrads of cells that result from deficient cell splitting. Scale bars, 1 μm.

C Frequency of cells in each cell cycle phase (see main text for description of phases) in wild-type strain NCTC8325-4 and knockout mutants 8325-4Δ*sle1* and 8325-4Δ*ftsK*, incubated with or without purified HisTag-Sle1$_{-SP}$. Note that accuracy in the quantification of cell cycle phases of the FtsK mutant in the background of strain NCTC8325-4 is impaired by overall agglomeration of cells. 2.7% of 8325-4Δ*ftsK* cells had abnormal morphologies and were not included in the graph. Data from three biological replicates of NCTC8325-4 (N_{total} = 728), 8325-4Δ*sle1* (N_{total} = 690), 8325-4Δ*sle1* + HisTag-Sle1$_{-SP}$ (N_{total} = 671), 8325-4Δ*ftsK* (N_{total} = 671); 8325-4Δ*ftsK* + HisTag-Sle1$_{-SP}$ (N_{total} = 689). Data presented in a stacked bars graph with each colored bar representing the mean percentage of cells in each cell cycle phase.

D SIM images of 8325-4Δ*sle1* and 8325-4Δ*ftsK S. aureus* cells incubated with purified HisTag-Sle1$_{-SP}$. External addition of the protein split the tetrads observed in *sle1* and *ftsK* knock-out strains. Scale bars, 1 μm.

E Transmission electron microscopy (TEM) images of 8325-4Δ*sle1* or 8325-4Δ*ftsK* cells showing a tetrad with a non-split septum from a first division, while a second round of division is already in progress. Scale bars, 500 nm.

this by purifying extracts containing surface proteins including autolysins (autolytic extracts) of 8325-4Δ*ftsK* and 8325-4Δ*sle1* mutants, in which noncovalently bound cell wall interacting proteins were extracted from cell pellets with SDS. Analysis of these autolytic extracts by Western blotting showed that Sle1 was absent from the cell surface of both mutants (Fig 2A). We also prepared cell wall

extracts by digesting the peptidoglycan with lysostaphin in the presence of sucrose, generating protoplasts and releasing to the supernatant peptidoglycan fragments and attached proteins. Sle1 was not present in the supernatant cell wall extracts of the 8325-4Δ*ftsK* mutant (Fig 2A).

Lack of Sle1 at the cell surface could be due to defects in any step of the Sle1 life cycle, from transcription, translation, export, to binding to the cell wall. Given that FtsK is a cytoplasmic protein lacking transmembrane domains, and with a DNA interacting C-terminal domain, we initially thought that FtsK could act as a transcriptional regulator of *sle1*. However, RNA sequencing showed that the levels of *sle1* transcript in 8325-4Δ*ftsK* are barely affected when compared to the parental strain NCTC8325-4 (1.6-fold decrease, *P*-value 0.14, not significant, Appendix Table S1).

An alternative hypothesis was that FtsK was required for the transport of Sle1 across the membrane and its export to the cell surface. If that was correct, Sle1 should accumulate in the cytoplasm of 8325-4Δ*ftsK* cells. However, analysis of protein extracts obtained from whole cells (total cellular extract) of the FtsK mutant showed no detectable Sle1 (Fig 2A). This was confirmed with total proteome analysis by mass spectrometry of the 8325-4Δ*ftsK* mutant, which verified the absence of FtsK and also showed no detectable Sle1 (Appendix Table S2), indicating that lack of FtsK was not impairing Sle1 transport and leading to its intracellular accumulation.

We then tested whether, in the absence of FtsK, Sle1 was produced and exported, but released to the growth medium instead of being targeted to the cell wall. For that, we collected and filtered the spent medium of cultures of 8325-4Δ*ftsK* and precipitated proteins with trichloroacetic acid (TCA). We could not detect any Sle1 protein in the spent medium of 8325-4Δ*ftsK* mutant either (Fig 2A).

Together these results show that 8325-4Δ*ftsK* mutant cells lack detectable levels of Sle1 in all cellular compartments.

FtsK-dependent Sle1 depletion requires the ClpXP proteolytic complex

After eliminating transcription, export, and attachment to the cell wall as the targets of FtsK-mediated Sle1 regulation, we questioned whether it could occur at the level of protein degradation. The first clue in this direction came from the selection of suppressor mutants in the 8325-4Δ*ftsK* background. While constructing this mutant, we inspected various of the obtained clones under the microscope and noticed that some lacked the daughter cell separation defects characteristic of the lack of FtsK. Whole genome sequencing of one of these clones, 8325-4Δ*ftsK**, identified three SNPs, one in the gene encoding the quinol oxidase polypeptide II QoxA (E273D), one in the gene encoding the Ribonuclease HII (A279V), and one which encoded a R95C substitution in the *clpX* gene. ClpX is an ATPase molecular chaperone that unfolds and translocates specific protein substrates, including Sle1, for degradation by ClpP proteolytic complexes (Frees *et al*, 2007; Olivares *et al*, 2016; Jensen *et al*, 2019). We showed that ClpX^{R95C} is a loss-of-function mutation, as it causes
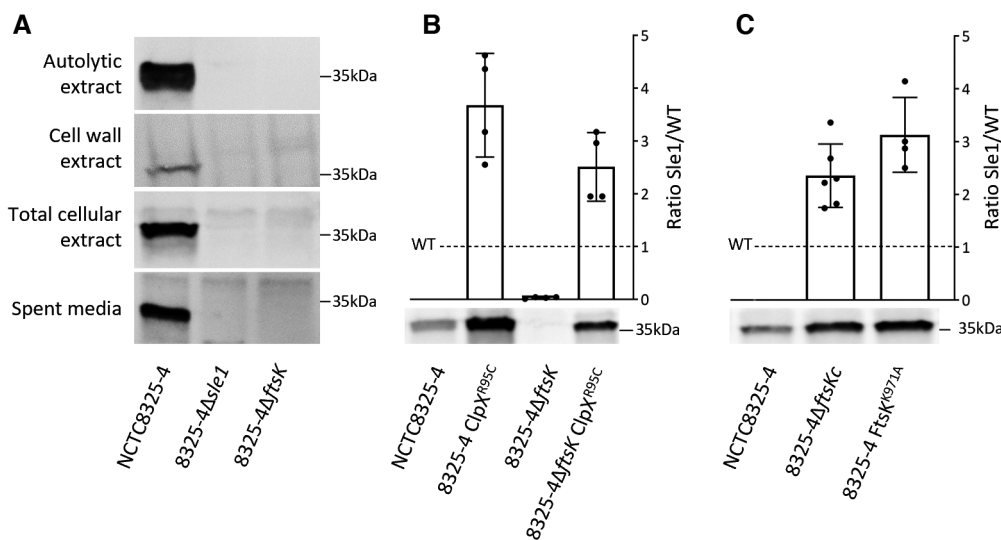

Figure 2. Sle1 is absent from all cellular compartments of FtsK mutant cells.

A   Absence of Sle1 in (from top to bottom) autolytic, cell wall or total cellular extracts and spent medium of 8325-4Δ*sle1* and 8325–4Δ*ftsK* mutants, but not in the parental strain NCTC8325-4, was confirmed by Western blot analysis using an anti-Sle1 antibody. All western blot experiments were performed with three biological replicates and representative images are shown.

B   Quantification of Sle1 total cellular levels, detected by western blot (representative gel on the bottom) in *S. aureus* mutant 8325-4Δ*ftsK* and ClpX inactivated mutants 8325-4 ClpX^{R95C} and 8325-4Δ*ftsK* ClpX^{R95C} showing that ClpX inactivation restores the presence of Sle1 in the *ftsK* deletion mutant.

C   Quantification of Sle1 total cellular levels, detected by western blot (representative gel on the bottom) in FtsK C-terminal deletion (8325-4Δ*ftsKc*) or inactivated (8325-4FtsK^{K971A}) mutants showing that Sle1 levels increase in the absence of FtsK DNA translocase activity.

Data information: Graphs show ratio between Sle1 amount in different samples versus the amount in parental strain NCTC8325-4 indicated by dashed line. Data represented in scatter dot plot column graphs, where column height represents mean, and error bars are the standard deviation. Data from at least four biological replicates. Source data are available online for this figure.

cold sensitivity and decreased extracellular proteolytic activity, previously described for *S. aureus* ClpX mutants (Frees *et al*, 2003; Appendix Fig S4A). Inactivation of ClpX should result in increased levels of Sle1, which was confirmed by Western blot analysis of total protein extracts of NCTC8325-4 and of 8325-4 ClpX^{R95C}, a mutant where the R95C-encoding mutation was introduced *de novo* in a clean NCTC8325-4 background (Fig 2B). We then compared Sle1 levels in 8325-4Δ*ftsK* (where Sle1 is undetectable) and 8325-4Δ*ftsK* ClpX^{R95C} and observed that Sle1 is present in this double mutant (Fig 2B), explaining why ClpX^{R95C} acts as a suppressor mutation for deletion of *ftsK* and why 8325-4Δ*ftsK* ClpX^{R95C} cells do not form tetrads (Appendix Fig S4B). However, 8325-4Δ*ftsK* ClpX^{R95C} cells are impaired in cell cycle progression as they have a longer phase 3 (Appendix Fig S4C). This suggests that (i) FtsK acts on Sle1 levels by directly or indirectly impairing its degradation by the ClpXP proteolytic machine and (ii) that the presence Sle1 is not sufficient to ensure normal cell cycle progression in the absence of FtsK.

Interestingly, both the walker A mutant 8325-4FtsK^{K971A}, with an inactivated DNA translocase domain, and the FtsK C-terminal deletion mutant 8325-4Δ*ftsKc*, which completely lacks the DNA translocase domain, show increased Sle1 levels (Fig 2C), similar to those observed in the ClpX mutants. Therefore, while the absence of FtsK leads to a disappearance of cellular Sle1, lack or inactivation of the DNA translocase domain leads to increased Sle1 levels, pointing to an important function of FtsK in the control of Sle1 levels.

In the presence of FtsK, trigger factor favors Sle1 export in the septal region, instead of degradation by ClpXP

A possible mechanism for the role of FtsK in preventing Sle1 degradation by ClpXP was a direct inhibition of ClpXP activity. However, this does not seem to be the case, because proteome analysis showed that the protein levels of 18 of 20 well-established ClpXP substrates (Feng *et al*, 2013) that were detected in the proteome of NCTC8325-4, were not appreciably altered (less than 1.5-fold) in 8325-4Δ*ftsK* (Appendix Table S2).

An alternative could be that FtsK interacted with Sle1, leading to its protection from degradation by ClpXP. We expressed a Sle1-FLAG fusion and performed immunoprecipitation, followed by mass spectrometry analysis to identify proteins interacting with Sle1. This approach did not detect FtsK as a possible Sle1 interaction partner. As it was possible that a FtsK–Sle1 interaction was mediated by a third protein, we decided to further analyze the list of proteins that co-immunoprecipitated with Sle1 (Appendix Table S3). Given that Sle1 is exported via the Sec pathway, it most likely has an unfolded conformation while in the cytoplasm. We therefore scanned the top 50 hits for chaperones involved in the Sec pathway and identified the trigger factor (TF) protein, encoded by the *tig* gene (Appendix Table S3). Trigger factor is a ubiquitous bacterial ribosome-docked chaperone that mediates the export of specific Sec-pathway substrates. We confirmed that Sle1 interacts with TF by performing co-immunoprecipitation assays using *S. aureus* extracts from strain 8325-4 TF-GFP expressing a green fluorescent protein (GFP) fusion to TF (Fig 3A).

We then tested whether TF interacted not only with Sle1, but also with FtsK. A bacterial two-hybrid assay, performed in *E. coli*, suggested that this interaction may take place and that it occurs via the N-terminal and/or linker domain of FtsK (Appendix Fig S5). An interaction between TF and FtsK was further confirmed in a co-immunoprecipitation assay (Fig 3B). More importantly, TF cellular localization in *S. aureus* cells was found to be dependent on the presence of FtsK: a GFP fusion to TF is distributed nonhomogenously in the cytoplasm of staphylococcal cells, forming a gradient that has higher concentrations in the septal region (Fig 4A and B, top). This gradient was maintained when TF-GFP was expressed in strain 8325-4Δ*ftsKc* that lacks the C-terminal domain of FtsK (Fig 4A and B, bottom) in agreement with the hypothesis that TF-FtsK interaction is mediated by FtsK N-terminal and/or linker domains. Strikingly, the TF-GFP gradient was lost in the absence of FtsK (Fig 4A and B, middle). We confirmed that this delocalization does not result from TF-GFP degradation (Appendix Fig S6). This suggests that TF can act as a chaperone that brings Sle1 to the septal region where FtsK is present, enriching Sle1 transport across the membrane in this region.

In the absence of TF, Sle1 protein is still present in the cell (Fig 5A). However, it is not exported at the correct location, as it can be seen more dispersed over the cell surface instead of mostly at midcell (Fig 5B). The Sec system is distributed over the entire cell membrane (Fig 5C), so in the absence of a specific localization mechanism, it is likely that Sle1 is exported by any Sec machinery, instead of being exported preferentially by those present at the septum. As a consequence, TF mutant 8325-4Δ*tig* cells have a delayed cell cycle phase 3, that is, cells take longer to split the division septum (Fig 5D). This shows that the tripartite interaction between Sle1, TF and FtsK is crucial for accurate spatial and possibly temporal control of Sle1 activity and consequently for timely completion of the cell cycle.

Sle1 levels are controlled in response to perturbations in chromosome replication/segregation

Why does FtsK, which has a major role in the early cell cycle process of chromosome segregation, control the levels of Sle1, a peptidoglycan hydrolase involved in the late cell cycle event of septum splitting? If cytokinesis was impaired due to a delay in chromosome segregation caused by the presence of chromosome dimers or DNA damage, but splitting of the division septum continued, then splitting of an incomplete septum would occur (Appendix Fig S7 ii). It is therefore possible that FtsK is involved in licensing initiation of septum splitting, so that this process is blocked if DNA replication/segregation is compromised (Appendix Fig S7 iii).

We tested whether Sle1 levels were decreased in conditions that cause DNA replication defects or DNA damage. For this, we grew cells in the presence of the DNA-damaging agent mitomycin C, or nalidixic acid, a fluoroquinolone antibiotic that targets DNA gyrase and topoisomerase IV, causing replication arrest. Western blot analysis of *S. aureus* cells grown in the presence of either compound showed that Sle1 levels are reduced to less than half when compared to cells grown in the absence of any antibiotic (Fig 6A). Furthermore, a delay in cell cycle phase 3 and the appearance of cell tetrads, phenotypes associated with impaired Sle1 function, were observed when bacteria were propagated in the presence of nalidixic acid (Fig 6B). The regulation of Sle1 levels is not mediated by the SOS response, as it still occurs in a mutant expressing the noncleavable S130A LexA variant (Appendix Fig S8). This mutant is unable
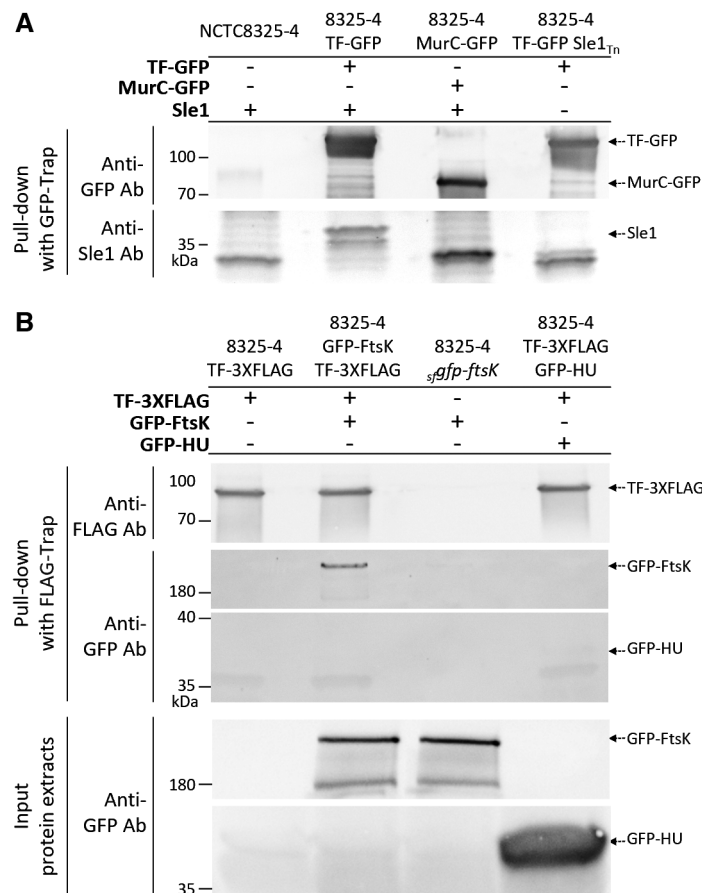
Figure 3. Trigger Factor (TF) interacts with Sle1 and FtsK.

A Total protein extracts of strains NCTC8325-4, 8325-4 TF-GFP, 8325-4 MurC-GFP and 8325-4 TF-GFP Sle1$_{Tn}$ (the latter lacking Sle1) were immunoprecipitated with GFP-Trap Magnetic Particles. Western blot analysis of the pulled-downed fractions using antibodies against Sle1 and GFP shows that Sle1 is pulled down with TF-GFP but not with negative control MurC-GFP, suggesting a specific interaction between TF and Sle1.

B Total protein extracts of strains 8325-4 TF-3XFLAG, 8325-4 GFP-FtsK TF-3XFLAG, 8325-4$_{sf}$*gfp-ftsK* and 8325-4 TF-3XFLAG GFP-HU (Input extracts, bottom panel) were immunoprecipitated with DYKDDDDK Fab-Trap Agarose that binds FLAG-tagged proteins. Western blot analysis of the pulled-downed fractions (top panels) using antibodies against FLAG and GFP shows that GFP-FtsK, but not the negative control GFP-HU, is pulled down with TF-3XFLAG, suggesting an interaction between TF and FtsK. For each assay, a representative image of three independent biological replicates is shown.

Source data are available online for this figure.

to induce the SOS response, as that requires autoproteolysis of the LexA repressor to derepress genes that are part of the SOS global regulatory network (Cirz *et al*, 2007).

We do not have direct evidence for a role of FtsK in the regulation of Sle1 levels in the presence of DNA-targeting agents. However, we noticed that the TF-GFP gradient, which leads to septal enrichment of TF and its Sle1 cargo, is lost in the presence of nalidixic acid (Fig 6C). Given that TF gradient is dependent on the presence of FtsK, one possible explanation for these results is that the interaction between FtsK and TF is impaired in these conditions, which would lead to loss of preferential export of Sle1 at the septal region, facilitating its degradation by ClpX.

Discussion

In *E. coli*, like in most Gram-negative bacteria, synthesis and splitting of the division septum take place in close succession, resulting in a gradual, coordinated, midcell constriction of all three envelope layers, the inner membrane, the peptidoglycan, and the outer membrane, during cytokinesis (Goehring & Beckwith, 2005). *S. aureus*, as well as other Gram-positive bacteria including the model organism *B. subtilis*, synthesize a complete septum before peptidoglycan hydrolases initiate septum splitting (Goehring & Beckwith, 2005). In some conditions, such as upon DNA damage or impaired chromosome replication/segregation, bacterial cells halt division to allow for repair while avoiding bisection of the nucleoid by a growing septum. The best studied mechanism mediating this process is the SOS response, which leads to inhibition of Z-ring formation or of later division proteins, allowing time for repair of damaged DNA (Mizusawa *et al*, 1983; Mukherjee *et al*, 1998; Modell *et al*, 2011; Bojer *et al*, 2019). It is conceivable that upon DNA damage, bacteria such as *S. aureus* have to halt not only septum synthesis, but also septum splitting. Failing to do so could lead to premature splitting of the septum, possibly exposing an immature cell
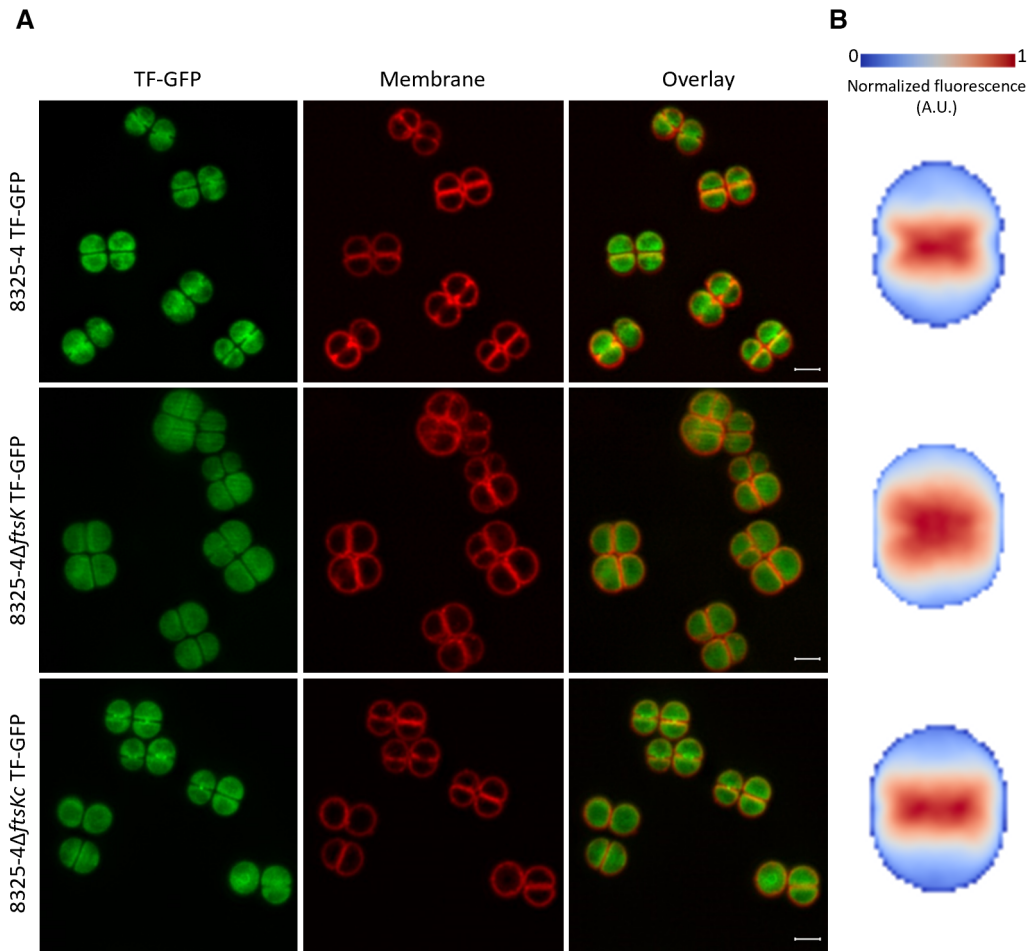
Figure 4.   Trigger Factor (TF) localization pattern is dependent on septal FtsK.

A   SIM images of cells expressing TF-GFP labeled with membrane dye FM5-95. TF-GFP forms a gradient towards the septum in the background of parental strain NCTC8325-4 (8325-4 TF-GFP, top panels). This localization pattern is lost in cells lacking FtsK (8325-4ΔftsK TF-GFP, middle panels), but not in 8325-4ΔftsKc TF-GFP mutant, expressing FtsK without its C-terminal domain (bottom panels). Scale bars, 1 μm.

B   Heatmap representation of TF-GFP average localization pattern in cells in phase 2 of the cell cycle (N = 50 for each strain). The color scale depicts the average normalized TF-GFP fluorescence signal in each pixel, ranging between 0 and 1. The fraction of the area of each cell model where the normalized signal intensity is above 70% of the maximum signal is 0.47, 0.68 and 0.48 for 8325-4 TF-GFP, 8325-4ΔftsK TF-GFP and 8325-4ΔftsKc TF-GFP, respectively, confirming that TF-GFP is enriched at midcell in the presence of FtsK and more dispersed over the cytoplasm in its absence.

surface, lacking surface proteins and glycopolymers that are essential virulence factors (Appendix Fig S7).

In this work, we have identified a mechanism for this newly recognized level of regulation, through which levels of the *S. aureus* peptidoglycan hydrolase Sle1, involved in septum splitting, are controlled by the key divisome protein FtsK. Notably, Sle1 becomes completely absent (undetectable by mass spectrometry) from *S. aureus* FtsK null mutant cells, due to degradation by the ClpXP proteolytic machinery. Protection of Sle1 degradation by FtsK is not mediated by direct interaction between the two proteins. We have shown that Sle1 interacts with TF, a chaperone that mediates the export of specific Sec-pathway substrates. TF, in turn, interacts with FtsK and becomes distributed in the cell in a gradient with higher concentrations near the septal region. Therefore, the concentration of TF's cargo, Sle1, will be higher near the Sec machineries present

in the septal region and lower near those at the peripheral membrane, leading to preferential export of Sle1 near the septum, where its activity is specifically required (Fig 6D, left). In the absence of FtsK, the TF gradient is dissipated, Sle1 is no longer preferentially exported at the septal region and becomes available for degradation by the ClpXP proteolytic machinery, leading to Sle1 depletion from the cell and delaying septum splitting (Fig 6D, right).

In *E. coli*, TF was shown to directly interact with ClpXP and to be the only chaperone capable of enhancing the degradation of some ClpXP substrates (Rizzolo *et al*, 2021). Phylogenetic and genome analyses showed that *tig* (encoding TF) is almost always located next to *clpX*, throughout the bacterial kingdom, including in Staphylococcaceae (Rizzolo *et al*, 2021), suggesting that a functional association between TF and ClpXP extends beyond *E. coli* (Rizzolo *et al*, 2021). We tried to detect an interaction between TF and ClpX
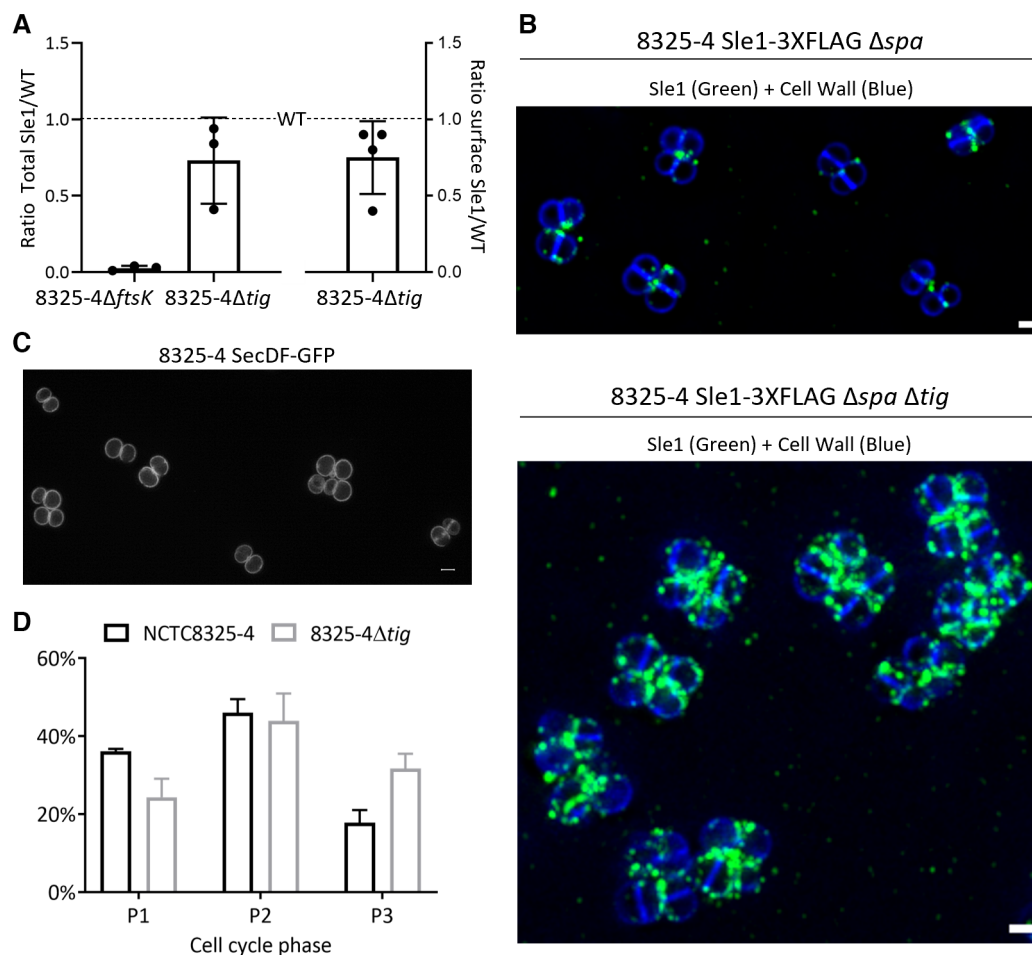
Figure 5. Absence of Trigger Factor (TF) alters Sle1 localization pattern, leading to impaired cell cycle progression.

A Quantification of Sle1 total cellular levels, detected by western blot, in *S. aureus* deletion mutants 8325-4Δ*ftsK* and 8325-4Δ*tig* and Sle1 surface levels in *tig* deletion mutant, showing that Sle1 is present at the cell surface in the absence of TF. Graph shows ratio between Sle1 amount in different samples versus the amount in parental strain NCTC8325-4 indicated by dashed line. Data represented in a scatter dot plot column graph, where column height represents mean, and error bars are the standard deviation. Data from at least three biological replicates.

B Deconvolved epifluorescence images of live cells of parental strain 8325-4 Sle1-3XFLAG Δ*spa* and TF deletion mutant 8325-4 Sle1-3XFLAG Δ*spa* Δ*tig*, producing Sle1-3XFLAG as the sole Sle1 copy in the cell. Normal localization pattern of Sle1 (enriched at midcell, top panel) is altered in the absence of TF (bottom panel) with the protein becoming more dispersed over the cell surface. See Appendix Fig S1 for more images of Sle1-3XFLAG surface localization in the parental strain and the negative control of the immunofluorescence assay. Cells were incubated with fluorescent D-amino acid HADA, which is incorporated into peptidoglycan, for cell wall visualization (colored blue). Cell surface Sle1-3XFLAG was detected with Anti-FLAG Monoclonal Antibody-Alexa Fluor 488 (colored green, projection of a 33 slices Z-stack shown). Scale bars, 1 μm.

C The machinery for Sec-mediated export is distributed over the entire cytoplasmic membrane. SIM image of the localization of SecDF-GFP functional fusion protein, expressed from *secDF* locus as the only SecDF copy in the cell, in strain 8325-4 SecDF-GFP. Scale bar, 1 μm.

D Frequency of cells in each cell cycle phase (see main text for description of phases) in the TF knockout mutant 8325-4Δ*tig* and NCTC8325-4 parental strain, showing that the TF mutant is delayed in cell cycle phase 3, taking longer to split the division septum. Data from three biological replicates of NCTC8325-4 (N_{total} = 728) and 8325-4Δ*tig* (N_{total} = 699). Data represented in column graphs where column height represents mean and error bars are the standard deviation.

in *S. aureus*, by bacterial two hybrid and co-immunoprecipitation, but were not successful. STRING analysis of protein–protein interaction networks (Szklarczyk *et al*, 2019) in *S. aureus* suggested that TF-ClpX interaction may be mediated by GroL or GroS chaperones. We therefore speculate that TF may have a double role in Sle1 regulation, preferentially bringing Sle1 to the septal region for localized export when a TF–FtsK interaction is established, and favoring Sle1 degradation by the ClpXP proteolytic machinery when the TF–FtsK interaction is lost.

This TF–FtsK-mediated mechanism to promote preferential export of Sle1 in the septal region is critical for normal progression of the cell cycle, as a mutant lacking TF, in which surface Sle1 is no longer enriched at the septum but is present over the cell surface (see Fig 5B), is impaired in cell cycle progression due to a delay in septum splitting.

In cells growing without antibiotics, a single-point mutation in the walker A motif of the C-terminal domain of FtsK, which abolishes its DNA translocase activity, as well as the deletion of the entire
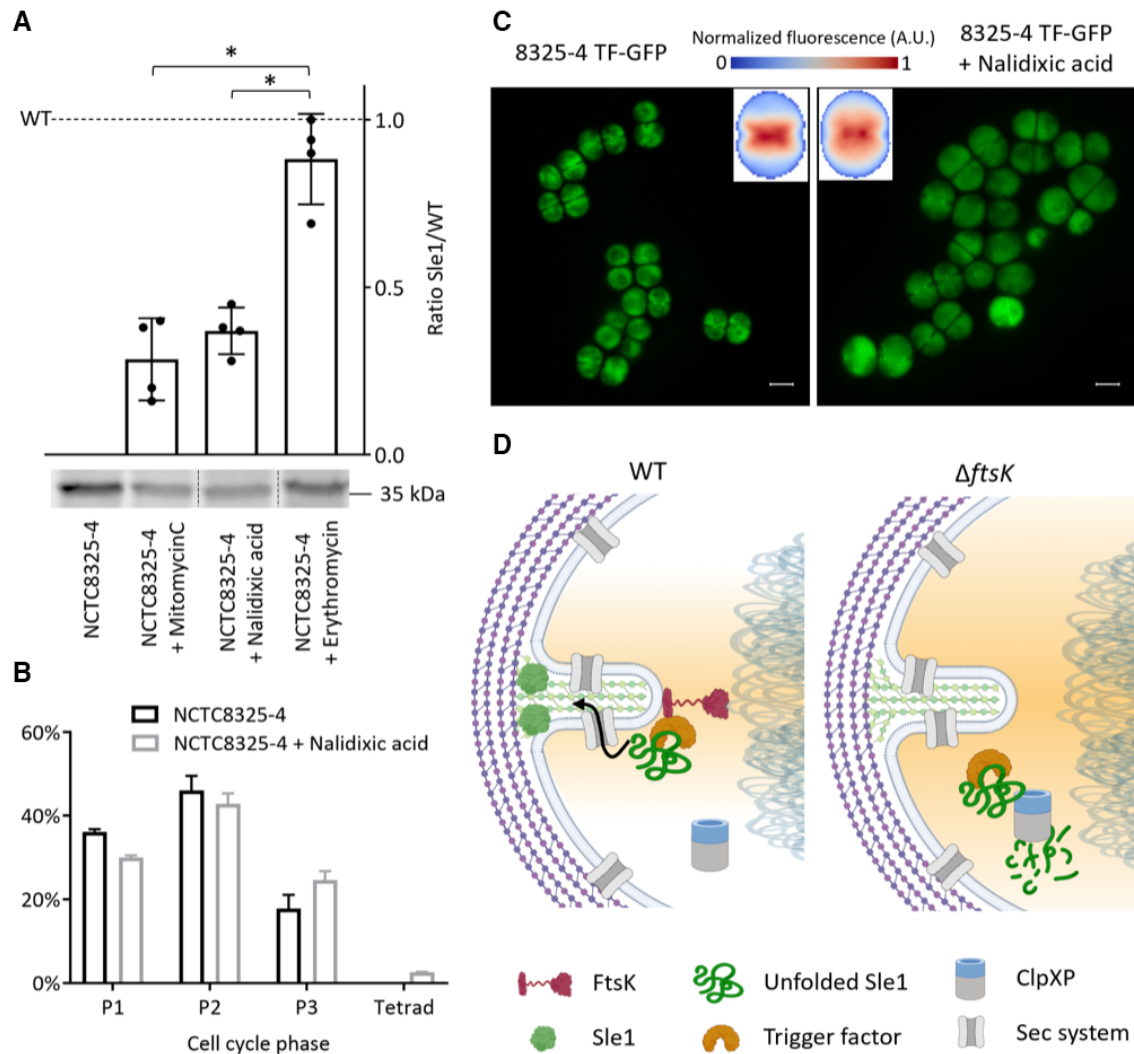
Figure 6. Sle1 levels are regulated in response to impaired chromosome replication/segregation.

A   Quantification of Sle1 total cellular levels, detected by western blot (representative gel on the bottom), in *S. aureus* cultures of wild-type strain NCTC8325-4 grown in the presence (1/2 X MIC) or absence of DNA targeting antibiotics mitomycin C and nalidixic acid or protein synthesis inhibitor erythromycin. The results show a decrease in Sle1 cellular levels upon DNA replication defects or DNA damage. Graphs show ratio between Sle1 amount in different samples versus the amount in parental strain NCTC8325-4 indicated by dashed line. Data represented in scatter dot plot column graphs, where column height represents mean, and error bars are the standard deviation. Data from four biological replicates. Statistical significance based on a Mann–Whitney *U* test, where *$P < 0.05$.

B   Frequency of cells in each cell cycle phase (see main text for description of phases) in *S. aureus* NCTC8325-4 cultures propagated in the presence or absence of nalidixic acid. The results show a delay in cell cycle phase 3 and the appearance of cell tetrads. Data from three biological replicates of NCTC8325-4 ($N_{total} = 728$) and NCTC8325-4 + nalidixic acid ($N_{total} = 700$). Data represented in column graphs where column height represents mean and error bars are the standard deviation.

C   SIM image and heat map representation of TF-GFP localization in 8325-4 TF-GFP cells grown in the presence or absence of nalidixic acid, showing the loss of TF-GFP gradient towards the septum in most cells grown in the presence of the antibiotic. Scale bars, 1 μm. Heatmaps represent the average of TF-GFP localization in 50 cells in phase 2 of the cell cycle. The color scale depicts the average normalized TF-GFP fluorescence signal in each pixel, ranging between 0 and 1. The fraction of the area of each cell model where the normalized signal intensity is above 70% of the maximum signal is 0.47 and 0.61 in the absence or presence of nalidixic acid, respectively, confirming that TF-GFP becomes more dispersed over the cytoplasm in the presence of the antibiotic.

D   Schematic representation of Sle1 regulatory mechanism mediated by the divisome protein FtsK. The secretory chaperone trigger factor binds unfolded Sle1 produced in the cytoplasm. In a wild-type strain (left panel), trigger factor interacts with FtsK, which localizes at the septum. This results in the establishment of a trigger factor concentration gradient towards the septal region (orange background) and favors preferential export of its cargo, Sle1, through the septal Sec-channels, in detriment of other channels positioned throughout the peripheral membrane. Additionally, it prevents Sle1 degradation by the ClpXP proteolytic machinery. The presence of folded Sle1 near septal peptidoglycan is necessary to promote timely daughter cells splitting. In the absence of FtsK (right-panel), the trigger factor gradient is dissipated and all Sle1 cellular protein is targeted for ClpXP degradation. DNA damage or impairment of chromosome replication/segregation also dissipates the trigger factor gradient, promoting Sle1 degradation by ClpXP. The consequent reduction of Sle1 levels halts septum splitting.

Source data are available online for this figure.

C-terminal domain, results in an approximately 2.5-fold increase in cellular Sle1 (Fig 2C). This is close to the Sle1 levels observed in the absence of Sle1 degradation by ClpX (Fig 2B). We speculate that during normal cell division, and in the absence of chromosomal dimers, translocation of DNA by FtsK ends upon the completion of chromosome segregation and that this may be a signal for the cell to initiate septum splitting, which would be promoted by increased Sle1 levels, equivalent to those observed in the 8325-4FtsK^{K971A} mutant where DNA translocase activity is abolished.

Hints for a role of FtsK in cell wall remodeling are present in the literature. FtsK has been proposed to interact with peptidoglycan synthesis proteins, based on bacterial two hybrid assays or mass spectrometry analysis, including with *E. coli* FtsI (PBP3; Di Lallo, 2003) or PBP1a (Berezuk *et al*, 2018), or *Streptococcus pneumoniae* FtsW (Maggi *et al*, 2008). Inactivation of FtsK in *E. coli* strains carrying large chromosomal inversions leads to aberrant cell morphology, reminiscent of defects in cells impaired in peptidoglycan synthesis (Lesterlin *et al*, 2008). *B. subtilis* SpoIIIE, an FtsK family protein, recruits PbpG during the asymmetric division that occurs when this bacterium undergoes sporulation (Mohamed *et al*, 2021). PbpG synthesizes peptidoglycan around the septal pore to counteract the activity of peptidoglycan hydrolases, contributing to the maintenance of a stabilized pore (Mohamed *et al*, 2021).

Here, we uncovered a direct role of FtsK in regulation of the levels of Sle1, a peptidoglycan hydrolase whose activity is critical for normal cell cycle progression in the bacterial pathogen *S. aureus*, providing a new link between the early and late steps of the bacterial cell cycle.

Materials and Methods

Bacterial strains and growth conditions

The bacterial strains and plasmids used in this study are listed in Appendix Tables S4 and S5, respectively. *Staphylococcus aureus* strains were grown in tryptic soy broth (TSB, Difco) or on tryptic soy agar (TSA, VWR), at 37°C or 30°C with aeration. *Escherichia coli* strains were cultured in Luria–Bertani broth (VWR) with aeration, or Luria–Bertani agar (VWR) at 37°C or 30°C. The growth medium was supplemented, when required, with 5-bromo-4-chloro-3-indolyl β-D-galactopyranoside (X-gal, 100 μg ml^{-1}, Apollo Scientific), isopropyl β-D-1-thiogalactopyranoside (IPTG, 0.1 or 0.5 mM, Apollo Scientific), ampicillin (100 μg ml^{-1}, Apollo Scientific), erythromycin (10 μg ml^{-1}, Apollo Scientific), and/or a combination of kanamycin (50 or 25 μg ml^{-1}, Apollo Scientific) with neomycin (50 or 25 μg ml^{-1}, Apollo Scientific).Plasmids were cloned and propagated in *E. coli* strains DC10B or DH5α.

Construction of *S. aureus* mutants

Primers used in this study are listed in Appendix Table S6.

For the deletion of *S. aureus*-native *phoB* gene in COL background, pMAD-Δ*phoB* plasmid was constructed. For that, *phoB* upstream and downstream regions (~ 1 Kb) were amplified from COL genome using the primers pairs P2002_phoB_EcoRI-F/P2003_phoB_OL-R and P2003_phoB_OL-F/P2005_phoB_bamHI-R, respectively. These two DNA fragments were then joined by overlap PCR with primers P2002_phoB_EcoRI-F and P2005_phoB_bamHI-R, and the resultant PCR product was digested with EcoRI and BamHI and cloned into pMAD vector, giving rise to pMAD-Δ*phoB*. The insert was sequenced and pMAD-Δ*phoB* was electroporated, as previously described (Veiga & Pinho, 2009), into RN4220 at 30°C (using erythromycin selection) and subsequently transduced to COL using phage 80α (Oshida & Tomasz, 1992). Strain COLΔ*phoB* was obtained after a two-step homologous recombination process. In the first step, recombinants in which the plasmids were integrated into the chromosome were selected at the nonpermissive temperature of 43°C. In the second step, recombinants in which the integrated plasmids (and consequently the *lacZ* and *erm* genes) had been excised were selected at the permissive temperature (30°C) in the absence of antibiotic selection. The *phoB* deletion was confirmed by PCR.

To screen for regulators of Sle1 presence at the cell outer surface, we constructed strain COLΔ*phoB* Sle1-phoB, which expresses a *sle1* fusion to *S. aureus* native *phoB* lacking the sequence encoding its signal peptide, as the only *sle1* copy in the cell and from the native chromosomal locus, in the background *phoB* deletion mutant. To substitute *sle1* for *sle1-phoB*$_{-SP}$ in COLΔ*phoB*, we used pMAD-Sle1PhoB plasmid that was constructed by first amplifying by PCR three DNA fragments: fragment 1 encompassing *sle1* 678 bp 3' end without the STOP codon; fragment 2 containing the sequence that encodes a 5aa linker and *phoB* lacking the sequence that encodes its first 30 amino acids (containing the signal peptide); and fragment 3 harboring *sle1* 672 bp downstream region. These three fragments were amplified from NCTC8325-4 genome using, respectively, the primer pairs UP SPsle1-sfGFP_P1_BamHI/Sle1PhoB_P2, Sle1PhoB_P3/Sle1PhoB_P4 and Sle1PhoB_P5/DOWN SPsle1-sfGFP_P6_SmaI and then joined by overlap PCR using primers SPsle1-sfGFP_P1_BamHI and DOWN SPsle1-sfGFP_P6_SmaI. The final PCR product was digested with BamHI and SmaI, cloned into pMAD to originate pMAD-Sle1PhoB and the insert was sequenced. This plasmid was electroporated into RN4220 at 30°C (with erythromycin selection), transduced to COLΔ*phoB*, followed by double crossover allelic exchange as described above. Colonies in which *sle1* was substituted for *sle1-phoB*$_{-SP}$ after pMAD-Sle1PhoB integration/excision were identified by PCR and named COLΔ*phoB* Sle1-phoB.

To construct a *spa* deletion mutant, the entire *spa* coding sequence was replaced by a 19 bp sequence harboring a NotI restriction site. For that, the 600 bp upstream and downstream regions of *spa* gene were amplified from NCTC8325-4 genome using, respectively, the primer pairs BCBP28/UP spa_NotI_P5 and DOWN spa_NotI_P6/BCBP29, with UP spa_NotI_P5 and DOWN spa_NotI_P6 introducing the 19 bp sequence mentioned above. The two amplified fragments were joined by overlap PCR with primers BCBP28 and BCBP29 and the final product was digested with BamHI and NcoI and cloned into pMAD vector, giving rise to pMAD-Δ*spa*. After confirming the correct sequence of the insert fragment, the plasmid was electroporated into RN4220 (selection with erythromycin, 30°C) and subsequently transduced to NCTC8325-4, using phage 80α. The replacement of *spa* for the 19 bp fragment with NotI restriction site, was obtained after integration and excision of pMAD-Δ*spa*, originating 8325-4Δ*spa*.

The ClpX and TF mutants were generated by deleting *clpX* and *tig* complete sequences from *S. aureus* genome. For that purpose, the upstream and downstream regions of each gene were amplified

by PCR, using for *clpX* the primers pairs ClpX_P1_BamHI/ClpX_P2 and ClpX_P3/ClpX_P4_SmaI and for *tig* the primer pairs Tig_P5_-BamHI/Tig_P2 and Tig_P3/Tig_P6_SmaI. The two PCR products for each deletion strategy were purified, joined in a second PCR using primers ClpX_P1_BamHI/ClpX_P4_SmaI for *clpX* and Tig_P5_-BamHI/Tig_P6_SmaI for *tig* and the resulting fragments were digested with BamHI and SmaI and cloned into pMAD. The resulting plasmids pMAD-Δ*clpX* and pMAD-Δ*tig*, for *clpX* and *tig* deletion, respectively, were sequenced, electroporated into RN4220 (selection with erythromycin) and subsequently transduced to NCTC8325-4, using phage 80α. After an integration/excision process, the deletion mutants 8325-4Δ*clpX* and 8325-4Δ*tig* were identified by PCR. Importantly, deletion of *tig* from *tig-clpX* locus did not interfere with the expression of its downstream gene *clpX*, as 8325-4Δ*tig* mutant is able to hydrolyse milk's casein.

Deletion of *ftsK* gene in COL background was obtained by first transducing plasmid pBCBHV012 (Veiga & Pinho, 2017) from RN4220 into COL. The integration of pBCBHV012, a pMAD-based plasmid containing *ftsK* up- and downstream regions, into the chromosome and its subsequent excision alongside *ftsK*, resulted in strain COLΔ*ftsK*.

Plasmids pMAD-ClpX^{R95C} and pMAD-LexA^{S130A} were constructed to introduce points mutations into *clpX* and *lexA* genes, respectively. pMAD-ClpX^{R95C} introduces a C to T alteration that causes a substitution of ClpX arginine 95 for a cysteine. This plasmid was constructed by amplifying a 2,281 bp fragment from the genome of strain *8325-4ΔftsK** that includes the R95C-encoding mutation acquired during the process of *ftsK* deletion and its upstream and downstream regions. For this PCR, primers ClpX_P1_BamHI and ClpX R95C_SmaI were used, and the amplified fragment was digested with BamHI and SmaI and cloned into pMAD. pMAD-LexA^{S130A} was designed to introduce an AG➜GC substitution that causes the alteration of LexA serine 130 to an alanine and was cloned by Gibson Assembly. For that, two PCR fragments containing the DNA sequences just upstream and downstream of the *lexA* point mutation site were amplified from NCTC8325-4 genome using primers pairs LexAS130A_P1/LexAS130A_P2 and LexAS130A_P3/LexAS130A_P4, with overlapping primers LexAS130A_P2 and LexAS130A_P3 including the desired bases substitution. SmaI linearized pMAD and the two amplified fragments were then mixed with Gibson Assembly Master Mix (NEB) and incubated at 50°C for 1 h according to the manufacturer's instructions, to obtain pMAD-LexA^{S130A}. The correct sequence of the inserts in pMAD-ClpX^{R95C} and pMAD-LexA^{S130A} was confirmed, and the plasmids were then introduced into RN4220 cells (30°C, erythromycin selection). Both plasmids were transduced into NCTC8325-4 and pMAD-ClpX^{R95C} was also transduced to 8325-4Δ*ftsK*. The substitution of *clpX* for *clpX*^{R95C} and *lexA* for *lexA*^{S130A}, in the different backgrounds, was obtained after a two-step homologous recombination process and was confirmed by sequencing. Final mutants were named 8325-4 ClpX^{R95C}, 8325-4Δ*ftsK* ClpX^{R95C} and 8325-4 LexA^{S130A}.

For localization of Sle1 by immunofluorescence and determination of Sle1 interaction partners through immunoprecipitation/mass spectrometry analysis we constructed strains 8325-4 Sle1-3XFLAG Δ*spa* and 8325-4 Sle1-3XFLAG* Δ*spa* that express Sle1 C-terminal fusions to the FLAG tag in the background of the *spa* deletion mutant, as the only Sle1 protein. In 8325-4 Sle1-3XFLAG Δ*spa*, Sle1 was fused to a 24 amino acids 3XFLAG peptide with three unaltered sequential FLAG epitopes (DYKDDDDKDYKDDDDKDYKDDDDK). In 8325-4 Sle1-3XFLAG* Δ*spa*, a shorter and altered 3XFLAG peptide with sequence DYKDHDGDYKDHDIDYKDDDDK was used. For the construction of these strains, we amplified from NCTC8325-4 genome, the 678 bp region upstream of *sle1* STOP codon and a 675 bp fragment encompassing *sle1* STOP codon and the downstream region. These two fragments were amplified by PCR using primers pairs UP SPsle1-sfGFP_P1_BamHI/Sle1FLAG_P10 and Sle1FLAG_P11/DOWN SPsle1-sfGFP_P6_SmaI with Sle1FLAG_P10 and Sle1FLAG_P11 containing the 3XFLAG sequence, or primers pairs UPSPsle1-sfGFP_P1_BamHI / SPSle1-FLAG_P7 and SPSle1-FLAG_P8/DOWNSPsle1-sfGFP_P6_SmaI which contain the coding sequence for 3XFLAG*. Each of the two pairs of fragments were then joined by overlap PCR giving rise to fragments *sle1* 3'-3XFLAG-down *sle1* and *sle1* 3'-3XFLAG*-down *sle1*, that were digested with BamHI and SmaI and cloned into pMAD, giving rise to, respectively, pMAD-Sle1-3XFLAG and pMAD-Sle1-3XFLAG*. Sequencing of the inserted fragments confirmed the correct sequence of *sle1* 3'-3XFLAG*-down *sle1* and showed that *sle1* 3' end and 3XFLAG sequences on *sle1* 3'-3XFLAG-down *sle1* have no alterations. However, a single nucleotide substitution in a noncoding region, 9 bp downstream of *sle1* STOP codon, was detected in *sle1* 3'-3XFLAG-down *sle1* fragment. pMAD-Sle1-3XFLAG and pMAD-Sle1-3XFLAG* vectors were electroporated into RN4220 (30°C, with erythromycin selection) and subsequently transduced to *spa* knockout mutant 8325-4Δ*spa*. The introduction of the tag sequence at *sle1* 3' end was obtained after an integration/ excision process, and confirmed by PCR and sequencing. The final strains were named 8325-4 Sle1-3XFLAG Δ*spa* and 8325-4 Sle1-3XFLAG* Δ*spa*. The localization of surface Sle1-3XFLAG in the absence of TF was observed by immunofluorescence in strain 8325-4 Sle1-3XFLAG Δ*spa* Δ*tig*. To construct this strain, the above described pMAD-Δ*tig* plasmid was introduced by transduction into 8325-4 Sle1-3XFLAG Δ*spa* and, following an integration/excision process, mutants with *tig* deletion were selected by PCR.

Plasmid pBCBSS135, encoding 3XFLAG-mNeonGreen fusion, was constructed by first amplifying a DNA fragment encoding 3XFLAG and a 5 aa linker, from complementary hybridized oligonucleotides 3xFLAG_oligo1 and 3xFLAG_oligo2, using primers RBS-3xFLAG_Sma_fwd and 5aa-linker-MCS-3xFLAG-rev. This PCR product was digested with SmaI and XhoI and cloned downstream of IPTG-inducible P*spac* promoter in pBCB13 (Pereira *et al*, 2010) vector. mNeonGreen sequence (codon-optimized for *S. aureus* by ATUM and synthesized by NZYtech) was then amplified using primers mNG_ + 4_Sal_fwd and mNG_EagI_rev, digested with SalI and EagI and cloned downstream of 3XFLAG sequence, generating pBCBSS135. The insert sequence was confirmed and pBCBSS135 was electroporated into RN4220 (30°C, erythromycin selection) and subsequently transduced to NCTC8325-4, giving rise to 8325-4 3xFLAG-mNG.

To construct *S. aureus* strains expressing a TF C-terminal FLAG tagged (DYKDDDDKDYKDDDDKDYKDDDDK) protein as the only TF in the cell, we constructed plasmid pMAD-TF-3XFLAG. For this, two DNA fragments encompassing *tig* 3' end and *tig* downstream region were amplified by PCR from NCTC8325-4 genome using, respectively, the primer pairs TigFLAG_P1_BamHI/Tig3FLAG_P2 and Tig3FLAG_P3/TigFLAG_P4_SmaI, containing the 3XFLAG sequence. A joint DNA fragment, *tig* 3'-3XFLAG- down *tig*, was then

generated by overlap PCR, digested with BamHI/SmaI, cloned into pMAD and its sequence confirmed by sequencing. pMAD-TF-3XFLAG vector was electroporated into RN4220 (30°C, with erythromycin selection) and subsequently transduced to wild-type strain NCTC8325-4 and 8325-4*sfgfp-ftsK* (Veiga & Pinho, 2017) that expresses GFP-FtsK as the only FtsK in the cell. The introduction of the FLAG tag sequence at *tig* 3′ end was obtained after an integration/excision process, confirmed by PCR and sequencing and the final strains were named, respectively, 8325-4 TF-3XFLAG and 8325-4 GFP-FtsK Sle1-3XFLAG.

Strain 8325-4 TF-3XFLAG GFP-HU, expressing, besides the TF FLAG fusion, a N-terminal sfGFP fusion to the DNA-binding protein HU, from *hup* locus and under the control of IPTG inducible promoter P_{spac}, was constructed by transducing the suicide vector pBCBPM030 (selection with Kanamycin/Neomycin) into the background of strain 8325-4 TF-3XFLAG.

pBCBPM030 was constructed by amplifying, from template vector pTrc99A-P7 (Fisher & DeLisa, 2008) and with primers PPMP1/PPMP2, an 800 bp DNA fragment encompassing $_{sf}gfp$ gene and the coding sequence for a 10 aa linker (TSGGGGSGGGGS) and, from NCTC8325-4 genome, a 500 bp DNA fragment containing *hup* gene, with primer pair PPMP3/PPMP4. These two fragments were joined by overlap PCR using primers PPMP1 and PPMP4, digested with EcoRI/BamHI and cloned into pBCBPM055.

pBCBPM055 vector is a derivative of pMUTIN4 plasmid (Vagner *et al*, 1998), where the erythromycin resistance gene was replaced for a kanamycin resistance marker obtained by PCR, from pBCBPM017 plasmid (Tan *et al*, 2012), using primers PPMP5 and PPMP6, and cloned with restriction enzymes NcoI and BglII.

To obtain *S. aureus* strains expressing C-terminal GFP fusions to MurC, TF and SecDF, plasmids pMAD-MurCGFP, pMAD-TFGFP, and pMAD-SecDFGFP were constructed. For the construction of pMAD-MurCGFP, three individual fragments were first amplified by PCR: fragment 1 encompassing the last 999 bp of *murC* gene (without STOP codon) was amplified from NCTC8325-4 genome using primers murCGFP_P1_BamHI and murCGFP_P2; 711 bp fragment 2, harboring a 5 aa linker and sfGFP encoding sequences, was amplified from template vector pTrc99A-P7 (Fisher & DeLisa, 2008) using primers murCGFP_P3 and murCGFP_P4 and fragment 3 harboring the 990 bp *murC* downstream region was amplified from NCTC8325-4 genome with primers murCGFP_P5 and murCGFP_P6_SmaI. The three fragments were then joined by overlap PCR, with primers murCGFP_P1_BamHI and murCGFP_P6_SmaI, the final product was digested with BamHI and SmaI and cloned into pMAD vector. Plasmids pMAD-TFGFP and pMAD-SecDFGFP were cloned by Gibson assembly. For the construction of pMAD-TFGFP, a first 1,283 bp DNA fragment, encompassing *tig* 3' end and the coding sequences for a 7 aa linker and sfGFP, was amplified using primer pair TigGFP_P1/TigGFP_P2 from pCNX-GFPc-TF plasmid, whose construction is described below and a second fragment, harboring *tig* 503 bp downstream region (including *clpX* 5′) was amplified from NCTC8325-4 genome with primers TigGFP_P3 and TigGFP_P4. For the construction of pMAD-SecDFGFP, a 1,293 bp DNA fragment, encompassing *secDF* 3' end, the coding sequences for a seven amino acid linker and sfGFP, was amplified using primer pair SecDFGFP_P1/ SecDFGFP_P2 from pCNX-GFPc-SecDF plasmid, whose construction is described below and a second fragment, harboring *secDF* 553 bp downstream region was amplified from

NCTC8325-4 genome with primers SecDFGFP_P3 and SecDFGFP_P4. A SmaI linearized pMAD and two fragments for each construct were then mixed with Gibson assembly master mix (NEB) and incubated at 50°C for 1 h according to the manufacturer's instructions. After cloning, pMAD-MurCGFP, pMAD-TFGFP, and pMAD-SecDFGFP constructs were confirmed by PCR, and the inserted fragments were sequenced. Plasmids were then introduced into electrocompetent *S. aureus* RN4220 cells (30°C, with erythromycin selection) and phage 80α was used to transduce pMAD-MurCGFP and pMAD-SecDFGFP into NCTC8325-4 and pMAD-TFGFP into NCTC8325-4, 8325-4Δ*ftsK* and 8325-4Δ*ftsKc*. The exchange of *murC*, *secDF* and *tig* genes for *murC*-$_{sf}gfp$, *secDF*-$_{sf}gfp$ and *tig*-$_{sf}gfp$, respectively, was obtained after an integration/excision process, as described above, and confirmed by PCR. The final strains were, respectively, named 8325-4 MurC-GFP, 8325-4 SecDF-GFP, 8325-4 TF-GFP, 8325-4Δ*ftsK* TF-GFP, and 8325-4Δ*ftsKc* TF-GFP. Importantly, the substitution of *tig* for *tig*-$_{sf}gfp$, did not interfere with the expression of *clpX* gene, located just downstream of *tig*, as *S. aureus* strains expressing TF-GFP are still able to hydrolyse milk's casein.

pCNX-GFPc plasmid was designed to facilitate cloning of GFP C-terminal fusions. For its construction, the coding sequence for a 5 aa linker and $_{sf}$GFP was amplified from pTrc99A-P7 (Fisher & DeLisa, 2008) using primers 5aa_sfGFP_SmaI and sfGFP STOP_EcoRI, digested with SmaI and EcoRI and cloned into pCNX plasmid. The insert was sequenced, and this vector served as backbone for the construction of plasmids pCNX-GFPc-TF and pCNX-GFPc-SecDF. For that, *tig* and *secDF* sequences (without their respective STOP codons) were amplified from NCTC8325-4 genome using, respectively, primers pairs Tig_Fw2_SmaI/ Tig_Rv2_SmaI and SecDF_C_P1_SalI/SecDF_C_P2_SmaI. The *tig* fragment was digested with SmaI, the *secDF* fragment was digested with SalI/SmaI and the digested fragments were then cloned into pCNX-GFPc upstream of *gfp*. The correct inserts sequences were confirmed.

Control strain 8325-4 TF-GFP Sle$_{Tn}$, harboring a *bursa aurealis* transposon (Tn) insertion at *sle1* coding sequence, was obtained through the transduction, using phage 80α, of *bursa aurealis* Tn from Nebraska Transposon Mutant Library mutant NE1688 (Fey *et al*, 2013) into the background of strain 8325-4 TF-GFP (erythromycin selection).

Transposon mutant library preparation and screening for mutants lacking Sle1 at *S. aureus* outer cell surface

A transposon mutant library was prepared in the background of strain COLΔ*phoB* Sle1-PhoB, following the protocol described by Wang *et al* (2011). For that, strains COLΔ*phoB* Sle1-PhoB pTM378 and COLΔ*phoB* Sle1-PhoB pTM381, expressing, respectively, an active or a truncated transposase (control), were first constructed, by transducing pTM378 or pTM381 plasmids into COLΔ*phoB* Sle1-PhoB (25 μg ml^{-1} kanamycin/25 μg ml^{-1} neomycin selection). Liquid cultures of these strains were then grown overnight at 30°C, rediluted, and grown the next morning until an OD$_{600nm}$ of 2 (~10^8 cfu ml^{-1}). At this point, 5 ml of cells were centrifuged at 3,000 *g* for 5 min and resuspended in an equal volume of SGMM medium (10 mM glucose; 2 mM MgCl$_2$; 3.5 mM CaCl$_2$; 0.1% Casein hydrolysate; 0.5% NaCl and 10 mM MES buffer pH 6.8). The cultures were infected with a 1:1:1 blend of three φ11 lysates carrying transposon cassettes with different promoters (MOI 2) and

incubated overnight without shaking at room temperature. Cells were then centrifuged at 3,000 *g* for 5 min, resuspended in 5 ml TSB, and incubated with gentle shaking at 37°C for 2 h. For identification of mutants that do not have Sle1-PhoB at the outer cell surface, the infected cultures were plated on TSA containing erythromycin 5 μg ml^{-1} (transposon selection) and PhoB substrate 5-Bromo-4-chloro-3′-indolyl phosphate p-toluidine (BCIP, 100 μg ml^{-1}) and incubated for 48 h at 37°C. White colonies were selected and the transposon insertion sites identified by inverted PCR.

Structured illumination microscopy (SIM) and cell cycle phases quantification

SIM imaging was performed using an Elyra PS.1 microscope (Zeiss) with a Plan-Apochromat 63×/1.4 oil DIC M27 objective. SIM images were acquired using five grid rotations, with 34 μm grating period for the 561 nm laser (100 mW), 28 μm period for 488 nm laser (100 mW), and 23 μm period for 405 nm laser (50 mW). Images were captured using a Pco.edge 5.5 camera and reconstructed using ZEN software (black edition, 2012, version 8.1.0.484) based on a structured illumination algorithm, using synthetic, channel-specific optical transfer functions and noise filter settings ranging from −6 to −8.

To evaluate *S. aureus* cells morphology and determine the percentage of population in each *S. aureus* cell cycle phase, cultures of NCTC8325-4 (in the presence or absence of 40 μg ml^{-1} nalidixic acid), 8325-4Δ*sle1*, 8325-4Δ*ftsK*, 8325-4Δ*ftsKc*, 8325-4FtsK^{K971A}, 8325-4Δ*ftsK* ClpX^{R95C}, 8325-4Δ*tig*, COL, COLΔ*sle1*, and COLΔ*ftsK* were grown at 37°C until OD$_{600nm}$ 0.65. At this point, 1 ml of culture was incubated for 5 min with the membrane dye Nile Red (Invitrogen, 2.5 μg ml^{-1}), the cells were harvested, resuspended in 20 μl of phosphate buffer saline (PBS), and placed on a microscope slide covered with a thin layer of agarose (1% in PBS) for SIM imaging.

To determine the ability of externally added Sle1 to complement Sle1 or FtsK absence, deletion mutants 8325-4Δ*sle1*, 8325-4Δ*ftsK* COLΔ*sle1*, and COLΔ*ftsK* were grown until OD$_{600nm}$ 0.3, the cultures were divided and grown with or without 7.5 μg ml^{-1} purified HisTag-Sle1$_{-SP}$ for an additional 30 min. The cells were labeled with Nile Red and prepared for SIM visualization as described above.

Following SIM image reconstruction, cells in each phase of *S. aureus* cell cycle were manually quantified. Cell cycle was divided in three phases: (P1) cells that have not initiated septum synthesis; (P2) cells undergoing septum synthesis; and (P3) cells with complete septum undergoing maturation prior to splitting. Cells with a tetrad phenotype can appear when a phase 3 cell does not complete septum splitting and a second round of division is initiated in the nonseparated daughter cells. Mutations that impair septum splitting, like the deletion of *sle1* or *ftsK* genes, in the background of fast-growing strains, like NCTC8425-4, have overall agglomeration of cells that makes cell cycle phases quantification less accurate. Final data represent the mean of three biological replicates.

The localization of SecDF-GFP and TF-GFP was visualized by SIM fluorescence microscopy. Strains 8325-4 SecDF-GFP, 8325-4 TF-GFP (in the presence or absence of 40 μg ml^{-1} nalidixic acid), 8325-4Δ*ftsK* TF-GFP and *8325-4Δ*ftsKc* TF-GFP* were grown at 37°C until OD$_{600nm}$ 0.65 and, when required, labeled for 5 min with membrane dye FM5-95 (Invitrogen, 5 μg ml^{-1}). Cells were then resuspended in

PBS and mounted on an agarose pad for SIM imaging, as described above.

Heatmaps of TF-GFP localization

The average TF-GFP localization pattern in cell cycle phase 2 cells of 8325-4 TF-GFP (in the presence or absence of 40 μg ml^{-1} nalidixic acid), 8325-4Δ*ftsK* TF-GFP and 8325-4Δ*ftsKc* TF-GFP strains was graphically represented as heatmaps. For that, crops of single cells in phase 2 ($N = 50$ for each strain) were generated using FIJI (Schindelin *et al*, 2012; Rueden *et al*, 2017) and, in each crop, pixels not corresponding to the respective cell were set to 0. A binary mask of each crop was generated by selecting the pixels only above a threshold calculated using the isodata algorithm (Velasco, 1980; van der Walt *et al*, 2014). The outline of each cell was calculated by performing binary erosion on the binary image and subtracting the original binary image by the eroded one. Cells were then aligned by first performing a Principal Components Analysis (PCA) on the outline coordinates to calculate the orientation of the major axis of each cell. Then, the angle of the major axis was calculated, and each single cell crop was rotated so that every cell has its major axis at a 90° angle. The average height and width of all cells was calculated, and each cell was resized to those values. The intensities of each cell image were normalized by setting the intensity range between 0 and 1, with 0 corresponding to the minimum intensity of each single cell crop and 1 corresponding to the maximum. To generate the average cell model, the normalized pixel intensities of all crops were averaged for each pixel with the same coordinates in every cell. Heatmaps were generated by calculating the background threshold using the isodata algorithm (Velasco, 1980; van der Walt *et al*, 2014) and setting the values below the threshold to white. Remaining pixels were colored by using the coolwarm colormap provided by the Python library matplotlib (Hunter, 2007), assigning the minimum and maximum of nonbackground intensity values of the cell models to the minimum and maximum values of the colormap.

Immunofluorescence of Sle1

Surface Sle1-3XFLAG was visualized by immunofluorescence of live, nonpermeabilized *S. aureus* cells. For that, strains 8325-4 Sle1-3XFLAG Δ*spa* and 8325-4 Sle1-3XFLAG Δ*spa* Δ*tig*, producing Sle1-3XFLAG as the sole Sle1 protein in the cell, and control strain 8325-4Δ*spa*, were grown until OD$_{600nm}$ 0.6, samples of 200 μl of each culture were centrifuged at 22,000 *g* for 1 min and cells were resuspended in an equal volume of sterile TSB in PBS solution (1/10). Fluorescent D-amino acid HADA was added to a final concentration of 250 μM and cells were incubated at 37°C for 30 min with agitation. A subsequent 5-min incubation with Conjugated DYKDDDDK Tag Monoclonal Antibody (L5)-Alexa Fluor™ 488 (Thermofisher Cat No. MA1-142-A488, 1:500 dilution) was performed for FLAG detection. Cells were then washed with PBS buffer and mounted on a microscope slide covered with a thin layer of agarose (1% in PBS). Z-stacks of 33 epifluorescence images with a Z step of 125 nm were acquired using a DeltaVision OMX SR microscope with an Olympus 60X PlanApo N/1.42 oil objective. The fluorophores were excited with a 488-nm laser (100 mW) and a 405-nm laser (100 mW). The software AcquireSRsoftWoRx (GE) was used for image acquisition and deconvolution.

Transmission electron microscopy

Cells of 8325-4Δ*sle1* and 8325-4Δ*ftsK* strains were observed by Transmission electron microscopy (TEM). Exponentially growing cultures of 8325-4Δ*sle1* and 8325-4Δ*ftsK* were harvested by centrifugation and cells were fixed with primary fixative solution (2.5% glutaraldehyde +1% osmium tetroxide in 0.1 M PIPES buffer at pH 7.2) for 1 h at 4°C, with gentle movement. Cells were then washed five times with MilliQ H$_2$O to remove the fixative and suspended in 3–4% agarose. Small sections of agarose-embedded cells were incubated overnight at 4°C in 0.5% uranyl acetate. The following day, samples were washed twice with MilliQ H$_2$O and dehydrated using 10-min steps in ethanol (30–100%), anhydrous ice-cold acetone, and anhydrous room temperature acetone. Samples were gradually shifted into 100% Spurr's resin and polymerized for 24 h at 60°C. Ultrathin sections (90 nm) were mounted on 200 mesh Cu grids and stained with Reynold's lead citrate. Excess stain was removed with degassed water and TEM imaging at 120 kV was performed on a FEI Tecnai 12 microscope, using a Gatan OneView CMOS camera with Digital Micrograph 3.0 software, at the Electron Microscopy Facility, Instituto Gulbenkian de Ciência, Oeiras, Portugal.

Isolation of *S. aureus* protein extracts

Surface proteins extracts (named autolytic extracts) and cell wall extracts, containing peptidoglycan attached proteins released upon protoplasts preparation, were obtained from 30 ml NCTC8325-4, 8325-4Δ*ftsK*, 8325-4Δ*sle1* and 8325-4Δ*tig S. aureus* cultures grown until OD$_{600nm}$ 0.65. Each culture was centrifuged at 3,000 *g*, for 15 min at 4°C. For purification of autolytic extracts, the cells were washed with WB buffer (50 mM Tris–HCl pH 7.5; 150 mM NaCl), resuspended in 200 μl of SDS 4% and incubated 30 min at 25°C with agitation. Cells were then harvested at 22,000 *g*, for 15 min, and the supernatant containing the autolytic extract was recovered. For isolation of protein cell wall extracts, cells were washed with DB buffer (1.2 M Sucrose; 50 mM Tris–HCl pH 7.5; 20 mM MgCl$_2$), resuspended in DB supplemented with 200 μg ml^{-1} lysostaphin, and incubated at 37°C for 1 h. Protoplasts were then pelleted at 6,000 *g* for 20 min, and the supernatant with cell wall proteins was recovered.

To obtain the spent media protein isolates, 90 ml NCTC832-5, 8325-4Δ*ftsK and* 8325-4Δ*sle1* cultures were grown until OD$_{600nm}$ 0.65, cells were harvested at 3000 *g* for 15 min, and the spent media was collected and filtered through a 0.22 μm pore size filter. The filtrate was then incubated overnight at 4°C with Trichloroacetic acid (TCA; one-tenth of the sample volume). Proteins were pelleted at 17,000 *g* for 15 min, the pellet was washed twice with ice-cold acetone, air-dried, and finally resuspended in 100 μl PBS buffer.

For the isolation of *S. aureus* total cellular extracts, 135 ml cultures was grown in TSB until OD OD$_{600nm}$ 0.65. To test the effect of antibiotics on Sle1 total cellular levels, NCTC8325-4 was grown in the presence of 0.4 μg ml^{-1} Mitomycin C, 40 μg ml^{-1} Nalidixic acid or 0.125 μg ml^{-1} Erythromycin and 8325-4 LexA^{S130A} in the presence of 0.2 μg ml^{-1} Mitomycin C (1/2 MIC). After growth, cells were harvested at 3,000 *g*, for 15 min, resuspended in 400 μl PBS buffer and mechanically broken using a SpeedMill Plus (Bioanalytik Jena; 3× 1 min cycles). Glass beads and cell debris were removed in two steps of 1 min 3,400 *g* centrifugation and the supernatant was

collected. The total protein content in the extracts was determined using the Bradford method and bovine serum albumin as a standard (BCA Protein Assay Kit, Pierce).

Imaging TF-GFP fluorescent protein in-gel

To analyze TF-GFP expression and integrity in strains 8325-4 TF-GFP and 8325-4Δ*ftsK* TF-GFP, 22 μg of these strains total protein cell extracts was loaded in a 12% Mini-Protean TGX pre-cast gel (Bio-Rad). Following protein separation, TF-GFP signal was detected using a FujiFilm FLA-5100 Fluorescent Image Analyzer and a 473 nm/LPB filter.

Western blot and quantification of Sle1 protein signal

Equal amounts of protein extracts were separated in 12% Mini-Protean TGX pre-cast gels (Bio-Rad) and then transferred to 0.2 μm nitrocellulose membranes using a Trans-Blot Turbo RTA Mini 0.2 μm Nitrocellulose Transfer Kit and Trans-Blot Turbo system (Bio-Rad). When Sle1 band quantification in total cell protein extracts was required, membranes were cut to separate the regions above and below ~40 KDa, and the bottom membrane (or complete membrane when only qualitative data were required) was blocked with 5% nonfat milk and incubated for 16 h with anti-Sle1 antibody (1:5,000 dilution). Sle1 was detected using Goat Anti-Rabbit IgG StarBright Blue 700 Fluorescent Secondary Antibody (Bio-Rad Cat No.12004161; 1:5,000 dilution) and an Invitrogen iBright Imaging System. To label all high-molecular weight proteins (in the top part of the cut membrane) or all proteins in each loaded extract, the membranes were incubated with Sypro-Ruby stain (Invitrogen) according to the manufacturer's instructions, and the dye signal was detected using the iBright Imaging System (Invitrogen). Invitrogen™ iBright™ Analysis Software was used to quantify the intensities of Sle1 and total Sypro-Ruby-stained bands. The intensity of each Sle1 protein band in a total cell extract was normalized against the total amount of high-molecular weight proteins in its own loaded extract. The intensity of Sle1 bands in the autolytic extracts was normalized against the total amount of Sypro-Ruby-stained proteins in total cell protein extracts of the same strain. The determined Sle1 signal for each sample was then normalized against the wild-type NCTC8325-4 Sle1 signal detected in the same protein membrane. GraphPad Prism 6 (GraphPad Software) was used to perform the statistical analysis. The differences in Sle1 total cellular levels between *S. aureus* cells treated with the control antibiotic erythromycin and cells treated with Mitomycin C or Nalidixic acid were evaluated with two-tailed Mann–Whitney *U* test. *P*-values < 0.05 were considered significant and were indicated with an asterisk.

Purification of HisTag-Sle1$_{-SP}$ and anti-Sle1 antibody production

To produce a recombinant Sle1 without its native signal peptide, we constructed plasmid pET21a-HisTag-Sle1$_{-SP}$. This plasmid was cloned by first amplifying, from the NCTC8325-4 genome, the *sle1* gene sequence without the first 5′ end 75 bp (encoding Sle1 signal peptide) using primers HisSle1_pETP4_NdeI and Sle1_pETP2_HindIII, with primer HisSle1_pETP4_NdeI introducing a 6XHis-tag encoding sequence at *sle1* 5′ end. The PCR product was then digested with NdeI and HindIII and cloned into pET21a vector, using

E. coli DH5α. The correct sequence of the insert was confirmed and pET21a-HisTag-Sle1_{-SP} transformed into competent *E. coli* BL21 (DE3) cells for protein expression.

A culture of BL21(DE3) pET21a-HisTag-Sle1_{-SP} was grown at 37°C with aeration in LB medium containing ampicillin 100 μg ml^{-1}. At OD$_{600nm}$ of 0.7, the culture was supplemented with 0.1 mM IPTG and grown for three additional hours. Cells were then collected by centrifugation at 4°C for 5 min at 13,000 *g*, the pellet was re-suspended at 4°C in buffer A (50 mM sodium phosphate buffer pH 8; 150 mM NaCl) supplemented with complete mini protease Inhibitor Cocktail (Roche) and DNase 10 μg ml^{-1}, and the cells were broken by performing two runs in a French Press at 1000 psi. The sample was centrifuged at 16,000 *g* for 20 min and the pellet containing inclusion bodies was resuspended in buffer B (50 mM sodium phosphate buffer pH 8; 300 mM NaCl) supplemented with 8 M urea. The suspension was incubated at 4°C with agitation until sample was homogeneous. At this point, an equal volume of buffer B was added to the sample to dilute urea to 4 M final concentration. After clarifying the sample of any insoluble debris by centrifugation at 16,000 *g* for 20 min, the sample was incubated with a preequilibrated HisTalon™ resin (Clontech) at 4°C with agitation for 30 min. Resin was recovered by spin-down centrifugation and washed first with Buffer B with 4 M urea and 10 mM imidazole followed by two washes without urea. The protein was eluted with Buffer B with 150 mM imidazole in a gravity flow column and the eluted fraction was dialyzed overnight against buffer A.

The protein sample was sent to COVALAB (France) for polyclonal antibody production in rabbits.

Co-immunoprecipitation/mass spectrometry analysis of Sle1 interaction partners

Co-immunoprecipitation was performed in triplicate for strain 8325-4 Sle1-3XFLAG* Δspa and in duplicate for control strain 8325-4 3xFLAG-mNG grown with aeration in 300 ml TSB medium, until OD$_{600nm}$ 0.6. Cultures of 8325-4 3xFLAG-mNG were supplemented with 0.1 mM IPTG. Cells were cooled on ice for 5 min, centrifuged 10 min at 7,200 *g*, and resuspended in 2 ml IP buffer (50 mM Tris pH 7.4; 150 mM NaCl; 5 mM EDTA; 5 mM MgCl$_2$; 25 mM sucrose; Complete Mini Protease Inhibitor Cocktail (Roche)). DNaseI (10 μg ml^{-1}, Sigma), RNaseA (20 μg ml^{-1}, Sigma), and lysostaphin (100 μg ml^{-1}, Sigma) were added to cell suspensions followed by incubation at 37°C for 1 h. Cell lysates were cooled on ice for 5 min and subsequently homogenized for 1 min in a SpeedMill Plus (Bioanalytik Jena). Glass beads and cell debris were removed in two centrifugation steps (each for 1 min at 3,400 *g*). Lysed cells were centrifuged 1 h at 21,000 *g*, and the supernatants were transferred to new reaction tubes containing equal volumes of IP buffer. Samples containing soluble proteins were incubated with 50 μl prewashed M2 affinity agarose (Sigma) at 4°C for 16 h with agitation. The resin was collected by centrifugation for 1 min at 5,000 *g*, washed eight times with 1 ml wash buffer (50 mM Tris pH 7.4; 150 mM NaCl), and bound proteins were eluted with 0.1 ml wash buffer containing 150 μg ml^{-1} 3xFLAG peptide (Sigma) for 15 min at room temperature. Western blot analysis was performed to verify presence of Sle1-3XFLAG* and 3xFLAG-mNG proteins in elution fractions. A volume 20 μl of

each fraction was loaded on 12% Mini-Protean TGX pre-cast gels (Bio-Rad) and gel slices containing co-immunoprecipitated proteins were isolated for subsequent analysis by mass spectrometry at Proteome Center Tübingen, Germany.

Pull-down assays

To test TF-Sle1 and TF-FtsK interactions, pull-down assays were performed using, respectively, the ChromoTek GFP-Trap magnetic agarose to pull-down GFP fusions and ChromoTek DYKDDDDK Fab-Trap Agarose to pull-down Flag-tagged proteins. Total cellular extracts of strains NCTC8325-4, 8325-4 TF-GFP, 8325-4 MurC-GFP, 8325-4 TF-GFP Sle1_{Tn}, 8325-4 TF-3XFLAG, 8325-4 GFP-FtsK TF-3XFLAG, 8325-4 _{sf}gfp-ftsK, and 8325-4 TF-3XFLAG GFP-HU (grown in the presence of 0.1 mM IPTG) were obtained from 270 ml cultures. For that, cultures were harvested at 3,000 *g*, for 15 min, the pellet was resuspended in Lysis buffer (1× TBS buffer pH 7.5; 10 μg ml^{-1} DNaseI; 20 μg ml^{-1} RNaseA; 100 μg ml^{-1} lysostaphin; 5 mM MgCl$_2$; Complete Mini Protease Inhibitor Cocktail tablet from Roche) and incubated with shaking at 37°C for 1 h. Samples were cooled on ice for 5 min and subsequently homogenized in a Speed-Mill Plus (Bioanalytik Jena, 3× 1 min cycles). The cells lysates were then centrifuged for 1 min three times (at 6,000, 13,000 and 18,000 *g*) to remove glass beads and cell debris. A 500 μl fraction of each cleared sample was mixed with 50 μl of pre-equilibrated GFP-Trap magnetic agarose (ChromoTek Cat No. gtma) or DYKDDDDK Fab-Trap Agarose (ChromoTek Cat No. ffa) and incubated overnight at 4°C rotating end-over-end. The beads were then washed twice with Wash buffer (10 mM Tris–HCl pH 7.5; 150 mM NaCl; 0.5 mM EDTA), resuspended in 2× SDS-Sample Buffer (120 mM Tris–HCl pH 6.8; 20% Glycerol; 4% SDS; 0.04% bromophenol blue; 10% β-mercaptoethanol), and boiled for 5 min. Western blot analysis was performed to verify the presence of GFP fusions in the pull-downed samples, using pabg GFP antibody rabbit polyclonal (Chromotek Cat No.50430-2-AP, 1:1,000 dilution), TF-3XFLAG protein, using Monoclonal anti-FLAG M2 mouse antibody (Sigma Cat No. F1804; 1:2,000 dilution), and Sle1 using a 1:5,000 dilution of anti-Sle1 antibody. For signal detection Goat Anti-Rabbit IgG StarBright Blue 700 fluorescent secondary antibody (Bio-Rad Cat No.12004161; 1:5,000 dilution) or Alexa-Fluor 594 goat anti-mouse IgG (H + L) secondary antibody (Invitrogen, Molecular Probes Cat No.A-11005; 1:2,000 dilution) and an Invitrogen iBright Imaging System, were used.

ClpX activity tests

ClpX activity in *S. aureus* strain 8325-4 ClpX^{R95C} and in the control strains NCTC8325-4 and 8325-4Δ*clpX* was tested by analyzing these strains sensitivity to cold (30°C) and their ability to hydrolyse milk's casein. NCTC8325-4, 8325-4 ClpX^{R95C} and 8325-4Δ*clpX* cultures were grown at 37°C until OD$_{600nm}$ 0.2, diluted, spotted on TSA plates and grown overnight at 30°C or 37°C. Overnight cultures of NCTC8325-4, 8325-4Δ*clpX* and 8325-4 ClpX^{R95C} were diluted 10^5-fold, plated on TSA containing 5% of skimmed milk, and grown overnight at 37°C. In the presence of an active ClpX, milk's casein is hydrolysed, forming a transparent halo around the colonies. Three independent experiments were performed.

Proteome analysis

For proteome analysis, strains NCTC8325-4 and 8325-4Δ*ftsK* were grown with shaking in 300 ml TSB medium, in triplicates, until the culture OD_{600nm} reached 0.6. A 50 ml fraction of each culture was cooled on ice for 5 min, cells were centrifuged for 10 min at 7,200 *g*, and resuspended in 0.5 ml PBS buffer supplemented with complete mini protease Inhibitor Cocktail (Roche). Cell suspensions were transferred to lysis tubes containing glass beads and subjected to mechanical disruption in a homogenizer SpeedMill Plus (Bioanalytik Jena) programed to six 1-min cycles. Glass beads and cell debris were removed in two steps of centrifugation each for 1 min at 3,400 *g*. Protein concentration in whole cell extracts was determined using Bradford reagent (Thermo Scientific), and 8 μg of total protein was loaded on 12% Mini-Protean TGX pre-cast gels (Bio-Rad). Gel slices containing whole cell extracts were isolated and analyzed by mass spectrometry at Proteome Center Tübingen, Germany. The MS data from all replicates were processed together using MaxQuant software suite v.1.5.2.8 (Cox & Mann, 2008). Database search was performed using the Andromeda search engine (Cox *et al*, 2011), which is integrated in MaxQuant. MS/MS spectra were searched against a target-decoy *Staphylococcus aureus* Uniprot database consisting of 799 protein entries and 245 commonly observed contaminants. In database search, full specificity was required for trypsin digest. Up to two missed cleavages were allowed. Carbamidomethylation of cysteine was set as fixed modification, whereas oxidation of methionine and acetylation of protein N-terminus were set as variable modifications. Initial mass tolerance was set to 4.5 parts per million (ppm) for precursor ions and 0.5 dalton (Da) for fragment ions. Peptide, protein, and modification site identifications were reported at a false discovery rate (FDR) of 0.01, estimated by the target/decoy approach (Elias & Gygi, 2007). Label-free algorithm were enabled, as was the "match between runs" option for samples within one biological replicate (Luber *et al*, 2010). Label-free quantification (LFQ) protein intensities from the MaxQuant data output were used for relative protein quantification. Downstream bioinformatic analysis (two-sample *t*-tests and Vulcano plots) was performed using the Perseus software package, version 1.5.0.15. Data were filtered for contaminants, reverse and only identified by site entries. Two sample tests were performed, considering $P < 0.05$ to be statistically significant and setting SO = 0.

RNA sequencing

To analyze NCTC8325-4 and 8325-4Δ*ftsK* transcriptomes, we extracted total RNA samples from three independent replicates of each of these strains. For that, NCTC8325-4 and 8325-4Δ*ftsK* cultures were grown until OD_{600nm} 0.6, cells were harvested, and RNA was extracted using Qiagen RNA Easy Kit. RNA samples were sent to CeGaT—Center for Genomics and Transcriptomics, Tuebingen, Germany, for library preparation and sequencing using an Illumina HiSeq platform (2×100 bp read length). Demultiplexing of the sequencing reads was performed with Illumina CASAVA (2.17). Reads quality was analyzed with FastQC (Andrews, 2010). Adapters were trimmed with Skewer (version 0.1.116; Jiang *et al*, 2014). Trimmed raw reads were aligned to NCTC8325 reference genome. Mapped reads were counted using HTSeq-count (version 0.6.1p1

with the additional options –i ID and –t gene; Anders *et al*, 2015). Analyses of differential expression between NCTC8325-4 and 8325-4Δ*ftsK* were performed with DESeq2 in R (Love *et al*, 2014). DESeq2 uses a negative binomial generalized linear model to test for differential expression based on gene counts.

Bacterial two hybrid assay

For bacterial adenylate cyclase two hybrid (BACTH) interaction studies, genes *tig*, *clpX*, *divIC*, *ftsK*, and the sequence encoding FtsK N-terminal and linker domains (*ftsK*$_{NL}$) were amplified from NCTC8325-4 genome and cloned into BACTH vectors pKNT25, pKT25, pUT18, and pUT18C (Karimova *et al*, 1998). PCR to obtain *clpX*, *divIC*, *ftsK*$_{NL}$ and *ftsK* were preformed using, respectively, the primers pairs ClpX_FW_XmaI/ClpX_BTH4_SacI, DivICBTH1_1bp-BamHI/DivICBTH2_KpnI, FtsKP7/FtsK NL_BTH4_SacI and FtsKP7/FtsK_BTH4_SacI. The obtained *clpX*, *ftsK*$_{NL}$ and *ftsK* DNA fragments were digested with XmaI/SacI and fused in-frame to the 5′ end of the *cyaA*$_{T25}$ gene in pKNT25, giving rise to pClpXT25, pFtsKT25 and pFtsK$_{NL}$T25, respectively. The *divIC* PCR product was digested with BamHI/KpnI and cloned in-frame with *cyaA*$_{T25}$ 3′ end in pKT25, generating pT25DivIC. Plasmid pFtsKT18 was also produced by cloning the above described *ftsK* DNA fragment in-frame with *cyaA*$_{T18}$ 5′ end in pUT18. PCR fragments encompassing *tig* and *clpX* genes were amplified using, respectively, primers pairs Tig_Fw3_1bpXbaI/Tig_Rv1_KpnI and ClpX_BTH1_BamHI/ ClpX_BTH2_KpnI_STOP and digested with XbaI/KpnI or BamHI/KpnI. The digested fragments were then cloned into pUT18C, in-frame with *cyaA*$_{T18}$ 3′ end, giving rise to, respectively, pT18TF and pT18ClpX. All inserted fragments were confirmed by sequencing. The resulting plasmids were initially obtained and propagated in *E. coli* DH5α and then different combinations were co-transformed in the reporter strain BTH101 (Karimova *et al*, 1998; cya-deficient) that was incubated at 30°C in LA containing 40 μg ml^{-1} X-Gal, 0.5 mM IPTG, 100 μg ml^{-1} ampicillin and 50 μg ml^{-1} kanamycin. ONPG (2-Nitrophenyl β-D-galactopyranoside) was used to assess the β-galactosidase activity of cell extracts obtained from liquid cultures of each co-transformed BTH101 strain, using the methodology described previously by Karimova *et al* (1998). β-galactosidase activity is expressed in Miller units where 1 Miller unit is equal to 1,000 $[(A_{420nm} - 1.75A_{550nm})/TVA_{600nm}]$ where T is the reaction time in minutes and V is the volume of culture assayed in milliliters. Data for each pair of T25 and T18 fused proteins results from 14 independent experiments. Statistical analysis was made using the GraphPad Prism software to calculate the *P*-values with two-tailed Mann–Whitney *U* test. Significant *P*-values were indicated with asterisks: **$P < 0.01$, ***$P < 0.001$ and ****$P < 0.0001$.

Data availability

Source code of Python scripts used for the analysis can be found in https://github.com/BacterialCellBiologyLab/CellAverager.

Strains and plasmids will be made available upon reasonable request.

Expanded View for this article is available online.

Author contributions

Helena Veiga: Conceptualization; resources; data curation; formal analysis; supervision; funding acquisition; validation; investigation; visualization; methodology; writing – original draft; project administration; writing – review and editing. **Ambre Jousselin:** Conceptualization; resources; investigation; methodology; writing – review and editing. **Simon Schäper:** Resources; formal analysis; investigation; methodology; writing – review and editing. **Bruno M Saraiva:** Software; validation; writing – review and editing. **Leonor B Marques:** Investigation; writing – review and editing. **Patricia Reed:** Investigation; writing – review and editing. **Joana Wilton:** Investigation; writing – review and editing. **Pedro M Pereira:** Resources. **Sérgio R Filipe:** Formal analysis; supervision; writing – review and editing. **Mariana G Pinho:** Conceptualization; formal analysis; supervision; funding acquisition; validation; writing – original draft; project administration; writing – review and editing.

Disclosure and competing interests statement

The authors declare that they have no conflict of interest.

References

Anders S, Pyl PT, Huber W (2015) HTSeq—a python framework to work with high-throughput sequencing data. *Bioinformatics* 31: 166–169

Andrews S (2010) FastQC: a quality control tool for high throughput sequence data. Available at http://www.bioinformatics.babraham.ac.uk/projects/fastqc

Aussel L, Barre FX, Aroyo M, Stasiak A, Stasiak AZ, Sherratt D (2002) FtsK is a DNA motor protein that activates chromosome dimer resolution by switching the catalytic state of the XerC and XerD recombinases. *Cell* 108: 195–205

Bartual SG, Straume D, Stamsas GA, Munoz IG, Alfonso C, Martinez-Ripoll M, Havarstein LS, Hermoso JA (2014) Structural basis of PcsB-mediated cell separation in *Streptococcus pneumoniae*. *Nat Commun* 5: 3842

Berezuk AM, Glavota S, Roach EJ, Goodyear MC, Krieger JR, Khursigara CM (2018) Outer membrane lipoprotein RlpA is a novel periplasmic interaction partner of the cell division protein FtsK in *Escherichia coli*. *Sci Rep* 8: 12933

Bi EF, Lutkenhaus J (1991) FtsZ ring structure associated with division in *Escherichia coli*. *Nature* 354: 161–164

Bigot S, Corre J, Louarn JM, Cornet F, Barre FX (2004) FtsK activities in Xer recombination, DNA mobilization and cell division involve overlapping and separate domains of the protein. *Mol Microbiol* 54: 876–886

Biller SJ, Burkholder WF (2009) The *Bacillus subtilis* SftA (YtpS) and SpoIIIE DNA translocases play distinct roles in growing cells to ensure faithful chromosome partitioning. *Mol Microbiol* 74: 790–809

Bojer MS, Wacnik K, Kjelgaard P, Gallay C, Bottomley AL, Cohn MT, Lindahl G, Frees D, Veening JW, Foster SJ *et al* (2019) SosA inhibits cell division in *Staphylococcus aureus* in response to DNA damage. *Mol Microbiol* 112: 1116–1130

Cirz RT, Jones MB, Gingles NA, Minogue TD, Jarrahi B, Peterson SN, Romesberg FE (2007) Complete and SOS-mediated response of *Staphylococcus aureus* to the antibiotic ciprofloxacin. *J Bacteriol* 189: 531–539

Cox J, Mann M (2008) MaxQuant enables high peptide identification rates, individualized p.p.b.-range mass accuracies and proteome-wide protein quantification. *Nat Biotechnol* 26: 1367–1372

Cox J, Neuhauser N, Michalski A, Scheltema RA, Olsen JV, Mann M (2011) Andromeda: a peptide search engine integrated into the MaxQuant environment. *J Proteome Res* 10: 1794–1805

Crane JM, Randall LL (2017) The sec system: protein export in *Escherichia coli*. *EcoSal Plus* 7: https://doi.org/10.1128/ecosalplus.ESP-0002-2017

Crozat E, Rousseau P, Fournes F, Cornet F (2014) The FtsK family of DNA translocases finds the ends of circles. *J Mol Microbiol Biotechnol* 24: 396–408

den Blaauwen T, Hamoen LW, Levin PA (2017) The divisome at 25: the road ahead. *Curr Opin Microbiol* 36: 85–94

Di Lallo G (2003) Use of a two-hybrid assay to study the assembly of a complex multicomponent protein machinery: bacterial septosome differentiation. *Microbiology* 149: 3353–3359

Egan AJF, Errington J, Vollmer W (2020) Regulation of peptidoglycan synthesis and remodelling. *Nat Rev Microbiol* 18: 446–460

Elias JE, Gygi SP (2007) Target-decoy search strategy for increased confidence in large-scale protein identifications by mass spectrometry. *Nat Methods* 4: 207–214

Feng J, Michalik S, Varming AN, Andersen JH, Albrecht D, Jelsbak L, Krieger S, Ohlsen K, Hecker M, Gerth U *et al* (2013) Trapping and proteomic identification of cellular substrates of the ClpP protease in *Staphylococcus aureus*. *J Proteome Res* 12: 547–558

Fey PD, Endres JL, Yajjala VK, Widhelm TJ, Boissy RJ, Bose JL, Bayles KW (2013) A genetic resource for rapid and comprehensive phenotype screening of nonessential *Staphylococcus aureus* genes. *mBio* 4: e00537-12

Fisher AC, DeLisa MP (2008) Laboratory evolution of fast-folding green fluorescent protein using secretory pathway quality control. *PLoS ONE* 3: e2351

Frankel MB, Schneewind O (2012) Determinants of murein hydrolase targeting to cross-wall of *Staphylococcus aureus* peptidoglycan. *J Biol Chem* 287: 10460–10471

Frees D, Qazi SN, Hill PJ, Ingmer H (2003) Alternative roles of ClpX and ClpP in *Staphylococcus aureus* stress tolerance and virulence. *Mol Microbiol* 48: 1565–1578

Frees D, Savijoki K, Varmanen P, Ingmer H (2007) Clp ATPases and ClpP proteolytic complexes regulate vital biological processes in low GC, gram-positive bacteria. *Mol Microbiol* 63: 1285–1295

Gibson CM, Caparon MG (2002) Alkaline phosphatase reporter transposon for identification of genes encoding secreted proteins in gram-positive microorganisms. *Appl Environ Microbiol* 68: 928–932

Goehring NW, Beckwith J (2005) Diverse paths to midcell: assembly of the bacterial cell division machinery. *Curr Biol* 15: R514–R526

Heilmann C, Hartleib J, Hussain MS, Peters G (2005) The multifunctional *Staphylococcus aureus* autolysin aaa mediates adherence to immobilized fibrinogen and fibronectin. *Infect Immun* 73: 4793–4802

Hunter JD (2007) Matplotlib: a 2D graphics environment. *Comput Sci Eng* 9: 90–95

Jensen C, Baek KT, Gallay C, Thalso-Madsen I, Xu L, Jousselin A, Ruiz Torrubia F, Paulander W, Pereira AR, Veening JW et al (2019) The ClpX chaperone controls autolytic splitting of *Staphylococcus aureus* daughter cells, but is bypassed by beta-lactam antibiotics or inhibitors of WTA biosynthesis. *PLoS Pathog* 15: e1008044

Jiang H, Lei R, Ding SW, Zhu S (2014) Skewer: a fast and accurate adapter trimmer for next-generation sequencing paired-end reads. *BMC Bioinformatics* 15: 182

Kaimer C, Gonzalez-Pastor JE, Graumann PL (2009) SpoIIIE and a novel type of DNA translocase, SftA, couple chromosome segregation with cell division in *Bacillus subtilis*. *Mol Microbiol* 74: 810–825

Kajimura J, Fujiwara T, Yamada S, Suzawa Y, Nishida T, Oyamada Y, Hayashi I, Yamagishi J, Komatsuzawa H, Sugai M (2005) Identification and molecular characterization of an N-acetylmuramyl-L-alanine amidase Sle1 involved in cell separation of *Staphylococcus aureus*. *Mol Microbiol* 58: 1087–1101

Karimova G, Pidoux J, Ullmann A, Ladant D (1998) A bacterial two-hybrid system based on a reconstituted signal transduction pathway. *Proc Natl Acad Sci USA* 95: 5752–5756

Lesterlin C, Pages C, Dubarry N, Dasgupta S, Cornet F (2008) Asymmetry of chromosome replichores renders the DNA translocase activity of FtsK essential for cell division and cell shape maintenance in *Escherichia coli*. *PLoS Genet* 4: e1000288

Levin PA, Janakiraman A (2021) Localization, assembly, and activation of the *Escherichia coli* cell division machinery. *EcoSal Plus* 9: eESP00222021

Liu Q, Cho H, Yeo WS, Bae T (2015) The extracytoplasmic linker peptide of the sensor protein SaeS tunes the kinase activity required for staphylococcal virulence in response to host signals. *PLoS Pathog* 11: e1004799

Love MI, Huber W, Anders S (2014) Moderated estimation of fold change and dispersion for RNA-seq data with DESeq2. *Genome Biol* 15: 550

Luber CA, Cox J, Lauterbach H, Fancke B, Selbach M, Tschopp J, Akira S, Wiegand M, Hochrein H, O'Keeffe M et al (2010) Quantitative proteomics reveals subset-specific viral recognition in dendritic cells. *Immunity* 32: 279–289

Maggi S, Massidda O, Luzi G, Fadda D, Paolozzi L, Ghelardini P (2008) Division protein interaction web: identification of a phylogenetically conserved common interactome between *Streptococcus pneumoniae* and *Escherichia coli*. *Microbiology* 154: 3042–3052

Manoil C, Mekalanos JJ, Beckwith J (1990) Alkaline phosphatase fusions: sensors of subcellular location. *J Bacteriol* 172: 515–518

Mizusawa S, Court D, Gottesman S (1983) Transcription of the *sulA* gene and repression by LexA. *J Mol Biol* 171: 337–343

Modell JW, Hopkins AC, Laub MT (2011) A DNA damage checkpoint in *Caulobacter crescentus* inhibits cell division through a direct interaction with FtsW. *Genes Dev* 25: 1328–1343

Mohamed AMT, Chan H, Luhur J, Bauda E, Gallet B, Morlot C, Cole L, Awad M, Crawford S, Lyras D et al (2021) Chromosome segregation and peptidoglycan remodeling are coordinated at a highly stabilized septal pore to maintain bacterial spore development. *Dev Cell* 56: 36–51

Monteiro JM, Fernandes PB, Vaz F, Pereira AR, Tavares AC, Ferreira MT, Pereira PM, Veiga H, Kuru E, VanNieuwenhze MS et al (2015) Cell shape dynamics during the staphylococcal cell cycle. *Nat Commun* 6: 8055

Mukherjee A, Cao C, Lutkenhaus J (1998) Inhibition of FtsZ polymerization by SulA, an inhibitor of septation in *Escherichia coli*. *Proc Natl Acad Sci USA* 95: 2885–2890

Olivares AO, Baker TA, Sauer RT (2016) Mechanistic insights into bacterial AAA+ proteases and protein-remodelling machines. *Nat Rev Microbiol* 14: 33–44

Oshida T, Tomasz A (1992) Isolation and characterization of a Tn*551*-autolysis mutant of *Staphylococcus aureus*. *J Bacteriol* 174: 4952–4959

Pereira P, Veiga H, Jorge A, Pinho M (2010) Fluorescent reporters for studies of cellular localization of proteins in *Staphylococcus aureus*. *Appl Environ Microbiol* 76: 4346–4353

Rizzolo K, Yu AYH, Ologbenla A, Kim SR, Zhu H, Ishimori K, Thibault G, Leung E, Zhang YW, Teng M et al (2021) Functional cooperativity between the trigger factor chaperone and the ClpXP proteolytic complex. *Nat Commun* 12: 281

Rueden CT, Schindelin J, Hiner MC, DeZonia BE, Walter AE, Arena ET, Eliceiri KW (2017) ImageJ2: ImageJ for the next generation of scientific image data. *BMC Bioinformatics* 18: 529

Saaki TNV, Teng Z, Wenzel M, Ventroux M, Carballido-Lopez R, Noirot-Gros MF, Hamoen LW (2022) SepF supports the recruitment of the DNA translocase SftA to the Z-ring. *Mol Microbiol* 117: 1263–1274

Schindelin J, Arganda-Carreras I, Frise E, Kaynig V, Longair M, Pietzsch T, Preibisch S, Rueden C, Saalfeld S, Schmid B et al (2012) Fiji: an open-source platform for biological-image analysis. *Nat Methods* 9: 676–682

Sham LT, Barendt SM, Kopecky KE, Winkler ME (2011) Essential PcsB putative peptidoglycan hydrolase interacts with the essential FtsXSpn cell division protein in *Streptococcus pneumoniae* D39. *Proc Natl Acad Sci USA* 108: E1061–E1069

Sherratt DJ, Arciszewska LK, Crozat E, Graham JE, Grainge I (2010) The *Escherichia coli* DNA translocase FtsK. *Biochem Soc Trans* 38: 395–398

Stouf M, Meile JC, Cornet F (2013) FtsK actively segregates sister chromosomes in *Escherichia coli*. *Proc Natl Acad Sci USA* 110: 11157–11162

Szklarczyk D, Gable AL, Lyon D, Junge A, Wyder S, Huerta-Cepas J, Simonovic M, Doncheva NT, Morris JH, Bork P et al (2019) STRING v11: protein-protein association networks with increased coverage, supporting functional discovery in genome-wide experimental datasets. *Nucleic Acids Res* 47: D607–D613

Tan CM, Therien AG, Lu J, Lee SH, Caron A, Gill CJ, Lebeau-Jacob C, Benton-Perdomo L, Monteiro JM, Pereira PM et al (2012) Restoring methicillin-resistant *Staphylococcus aureus* susceptibility to β-lactam antibiotics. *Sci Transl Med* 4: 126ra135

Uehara T, Parzych KR, Dinh T, Bernhardt TG (2010) Daughter cell separation is controlled by cytokinetic ring-activated cell wall hydrolysis. *EMBO J* 29: 1412–1422

Vagner V, Dervyn E, Ehrlich SD (1998) A vector for systematic gene inactivation in *Bacillus subtilis*. *Microbiology* 144: 3097–3104

van der Walt S, Schonberger JL, Nunez-Iglesias J, Boulogne F, Warner JD, Yager N, Gouillart E, Yu T, Scikit-Image Contributors (2014) Scikit-image: image processing in python. *PeerJ* 2: e453

Veiga H, Pinho MG (2009) Inactivation of the SauI type I restriction-modification system is not sufficient to generate *Staphylococcus aureus* strains capable of efficiently accepting foreign DNA. *Appl Environ Microbiol* 75: 3034–3038

Veiga H, Pinho MG (2017) *Staphylococcus aureus* requires at least one FtsK/SpoIIIE protein for correct chromosome segregation. *Mol Microbiol* 103: 504–517

Velasco F (1980) Thresholding using the ISODATA clustering algorithm. *IEEE Trans Syst Man Cybern* 10: 771–774

Vollmer W, Joris B, Charlier P, Foster S (2008) Bacterial peptidoglycan (murein) hydrolases. *FEMS Microbiol Rev* 32: 259–286

Wang H, Claveau D, Vaillancourt JP, Roemer T, Meredith TC (2011) High-frequency transposition for determining antibacterial mode of action. *Nat Chem Biol* 7: 720–729

Zhou X, Halladin DK, Rojas ER, Koslover EF, Lee TK, Huang KC, Theriot JA (2015) Bacterial division. Mechanical crack propagation drives millisecond daughter cell separation in *Staphylococcus aureus*. *Science* 348: 574–578